Geometric, kinematic, and erosional history of the central Andean Plateau, Bolivia (15–17°S)

Nadine McQuarrie,[1] Jason B. Barnes,[2] and Todd A. Ehlers[2]

Received 2 October 2006; revised 5 December 2007; accepted 7 January 2008; published 28 May 2008.

[1] Latitudinal changes in topography, climate, and thrust belt geometry in the central Andes have led to conflicting hypotheses that climate or tectonics exert a first-order control on orogen evolution. The relative roles of climate and tectonics in the evolution of the Andean orogen are difficult to quantify because of a lack of detailed observations for both the long-term deformation and erosion history of the Andean fold-thrust belt. We contribute to the resolution of this problem by presenting a sequentially restored, balanced cross section based on new mapping across the northern Bolivia portion of the thrust belt (15–17°S). The timing and magnitude of exhumation across the cross section are determined by synthesizing 10 new and ~70 previously published mineral cooling ages. Once balanced and restored, the section was sequentially forward modeled using stratigraphic and cooling age constraints. Results indicate the Eastern Cordillera (EC) records the highest magnitudes of shortening (123 km or 55%). The Interandean zone (IA) has shortened 48 km or 30%. In both the EC and IA individual thrust sheets are tightly folded and have minor offsets of 1–5 km. The Subandes (SA) has multiple levels of detachments allowing for thrust sheets with relatively large offsets (6–17 km). Total shortening in the SA is 66 km or 40%. Total magnitude of shortening for the entire fold-thrust belt in this region is 276 km (40%). New apatite and zircon fission track cooling ages in conjunction with published ages indicate two phases of rapid exhumation; an earlier phase from ~40 to 25 Ma in the EC and one prior to ~25 Ma in the IA, followed by distributed exhumation of the entire fold-thrust belt from ~15–0 Ma. Combined exhumation estimates from the balanced cross section and thermochronology suggest ~9–11 km of exhumation in the EC, ~5–9 km in the IA, and ~3–4 km in the SA. Long-term shortening rates are 7 mm/a for the EC and IA and 4–8 mm/a for the SA. The SA shortening rates are based on a ~15–0 Ma or 8–0 Ma deformation window. By linking cooling ages to location and magnitude of shortening, we suggest an ~10–17 Ma pause or a dramatic deceleration in the rate of deformation and propagation of the fold-thrust belt between 25 and ~15 or 8 Ma. **Citation:** McQuarrie, N., J. B. Barnes, and T. A. Ehlers (2008), Geometric, kinematic, and erosional history of the central Andean Plateau, Bolivia (15–17°S), *Tectonics*, *27*, TC3007, doi:10.1029/2006TC002054.

1. Introduction

[2] It has been hypothesized that climate-driven variations in erosion may localize exhumation and deformation in mountain ranges thereby influencing the style and location of deformation as well as the morphology [*Avouac and Burov*, 1996; *Beaumont et al.*, 1992; *Dahlen and Suppe*, 1988; *Hodges et al.*, 2004; *Montgomery et al.*, 2001; *Stolar et al.*, 2006; *Willett*, 1999; *Zeitler et al.*, 1993]. The Andes mountains in South America are often used to illustrate variations in deformation, exhumation and morphology that are thought to be due to significant along strike changes in climate [*Horton*, 1999; *Lamb and Davis*, 2003; *Masek et al.*, 1994; *Montgomery et al.*, 2001]. However, in order for geodynamical models to test the magnitude of coupling between climate and tectonics along the Andean mountain chain, the kinematic and erosional history of the mountain range must first be quantified independently.

[3] Previous studies have addressed the interplay of climate and tectonics in the central Andes using large-scale geomorphic indices [*Montgomery et al.*, 2001], synthesis of modern and ancient denudation rates and magnitudes [*Barnes et al.*, 2006; *Barnes and Pelletier*, 2006; *Ege et al.*, 2007; *Horton*, 1999], and numerical modeling [*Babeyko et al.*, 2006; *Masek et al.*, 1994; *Sobolev et al.*, 2006]. Detailed studies of long-term deformation in the central Andes have documented the magnitude and geometry of shortening of the Andean Plateau and adjacent fold-thrust belt from 17°S to 21°S [*Kley*, 1996; *McQuarrie and DeCelles*, 2001; *Müller et al.*, 2002; *McQuarrie*, 2002; *Elger et al.*, 2005]. These structural studies have highlighted the need for systematic data on the age of both deformation and exhumation to constrain the tempo of deformation as well as exploit genetic links between the evolution of the fold-thrust belt and the development of the Andean Plateau. Several recent studies in southern Bolivia [*Barnes et al.*, 2008; *Ege et al.*, 2007; *Elger et al.*, 2005] and northern Bolivia [*Barnes et al.*, 2006; *Gillis et al.*, 2006] have begun to fill this data gap by linking geochronologic and thermochronologic data to structural cross sections.

[1]Department of Geosciences, Princeton University, Princeton, New Jersey, USA.
[2]Department of Geological Sciences, University of Michigan, Ann Arbor, Michigan, USA.

0278-7407/08/2006TC002054$12.00

[4] We complement and add to the previous studies by presenting new mapping and an associated balanced cross section through the Beni drainage basin of the central Andes (15–17°S) (Figure 1). The Beni drainage basin provides some of the most dramatic topography of the central Andes and dominates sediment input to the southern Amazon basin [*Aalto et al.*, 2006; *Dunne et al.*, 1998; *Masek et al.*, 1994]. It is also associated with a pronounced low-elevation indentation in the topography of the fold-thrust belt (Figure 2) [*Isacks*, 1988; *Montgomery et al.*, 2001]. This study describes (1) new mapping to characterize the structural style within the Rio Beni drainage basin, (2) a sequentially restored balanced cross section to constrain shortening estimates, geometry and large-scale kinematics of the Andes in northern Bolivia, (3) new and previously published mineral cooling ages to determine the timing of rock cooling across the balanced section, and (4) the kinematic history of deformation across the region. The kinematic history was created under the assumption that initiation of motion on faults generates relief and associated erosional exhumation, and that the exhumation is recorded in the cooling ages. Integration of the cross section with mineral cooling ages constrains the magnitude of exhumation in the fold-thrust belt as well as the timing and rates of deformation.

2. Background

2.1. Geologic Setting

[5] The central Andes house two of South America's most distinguishing features, a pronounced seaward concave bend of the western coast and cordillera and the ~4-km-high Andean Plateau (Figure 1). The axis of the oroclinal bend effectively divides the central Andes into a wide (~550 km), dry southern portion and a narrower (400–450 km), wetter northern portion. The central Andean Plateau, as defined by a broad area of internally drained basins and moderate relief with an average elevation of ≥3 km [*Isacks*, 1988], also varies in width from north to south (Figures 1a and 1d). The western edge of the plateau is marked by the 6- to 6.5-km-high volcanic peaks of the Western Cordillera. The equally high peaks of the Eastern Cordillera (EC) are composed of folded and faulted Paleozoic rocks in the hinterland of the Andean fold-thrust belt. Between the two cordilleras is the broad (~200 km wide) 3.8-km-high internally drained basin of the Altiplano. East of the EC, elevations descend into the Interandean zone (IA), with elevations between 1 and 2 km, followed by the frontal, active, Subandes (SA) with elevations less than 1 km grading into the foreland (Figure 1a).

[6] In northern Bolivia, the Beni drainage system has breached the Eastern Cordillera and is actively draining a portion of the Altiplano (Figure 1b). Rio La Paz, Rio Luribay and Rio Sapahaqui, tributaries to the Rio Beni, have exhumed most of the Quaternary through Tertiary basin sediments that once covered a significant portion (~5300 km^2) of the fold-thrust belt within the Altiplano basin (Figures 1 and 2). Exhumation of this area exposed a wide, west verging portion of the fold-thrust belt and the structural transition between the Paleozoic rocks within the EC and the thick Tertiary sediments preserved in the Altiplano (Figures 1 and 2 and Foldout 1) [*McQuarrie and DeCelles*, 2001].

[7] The sedimentary cover rocks involved in the Andean fold-thrust belt are a thick (~12–15 km), continuous succession of Paleozoic marine siliciclastic strata, a thinner, discontinuous section (2–4 km) of nonmarine Carboniferous through Cretaceous rocks [*Gonzalez et al.*, 1996; *Roeder and Chamberlain*, 1995; *Sempere*, 1995; *Sempere et al.*, 1994], and locally thick sections (up to 12 km thick within the Altiplano) of Tertiary synorogenic sedimentary rocks [*Horton et al.*, 2001; *Lamb and Hoke*, 1997; *Sempere et al.*, 1990]. The thickest part (~15 km) of the Paleozoic succession is centered in the EC [*Roeder and Chamberlain*, 1995; *Sempere*, 1995; *Welsink et al.*, 1995] and tapers eastward onto the Brazilian shield [*Welsink et al.*, 1995] and westward toward the Altiplano [*Roeder and Chamberlain*, 1995; *Sempere*, 1995]. The fold-thrust belt is bivergent in the central Andes. The axis of vergence in the upper crustal rocks is centered in the EC [*Baby et al.*, 1997; *McQuarrie*, 2002; *McQuarrie and DeCelles*, 2001; *Roeder*, 1988; *Roeder and Chamberlain*, 1995; *Sempere et al.*, 1990] with an extensive west verging back thrust system extending from the high peaks of the EC into the Altiplano to the west. Although late Paleozoic pre-Andean deformation has been documented in southern most Bolivia (21°S) [e.g., *Müller et al.*, 2002], the presence of conformable Jurassic and younger strata on Paleozoic strata exposed in numerous synclines throughout the EC from 20°S to 17°S indicates that ~20.5°S is the northern limit of pre-Andean deformation in Bolivia [*Sempere*, 1995; *McQuarrie and Davis*, 2002]. The lack of pre-Andean deformation from 17 to 15°S is supported by the presence of conformable Carboniferous through Cretaceous strata preserved in topographically perched synclines through the Rio Beni drainage basin (Foldout 1) and remarkably similar structural patterns of Andean deformation from 15 to 21°S [*McQuarrie*, 2002; *McQuarrie and DeCelles*, 2001; *Müller et al.*, 2002].

2.2. Previous Chronology

[8] Previous thermochronolgy and geochronology studies in northern Bolivia have provided information on the timing of rock cooling for portions of the thrust belt. Previous fission track studies in northern Bolivia focused on Triassic plutons of the Eastern Cordillera located adjacent to the plateau margin (Figures 1b and 1c) [*Benjamin*, 1986; *Crough*, 1983; *Guarachi et al.*, 2001; *Safran*, 1998; *Safran et al.*, 2006]. Combined U-Pb, ^{40}Ar/^{39}Ar, and apatite and zircon fission track data of some of the same and adjacent plutons record ~10 km erosion-related exhumation in the Eo-Oligocene and from late Miocene to present [*Gillis et al.*, 2006]. The previous studies all suggest shortening began ~40 Ma in the northern EC [*McQuarrie*, 2002; *McQuarrie et al.*, 2005]. Subandes deformation in northern Bolivia is inferred to be Neogene based on limited ages constraints on the foreland basin chronostratigraphy and

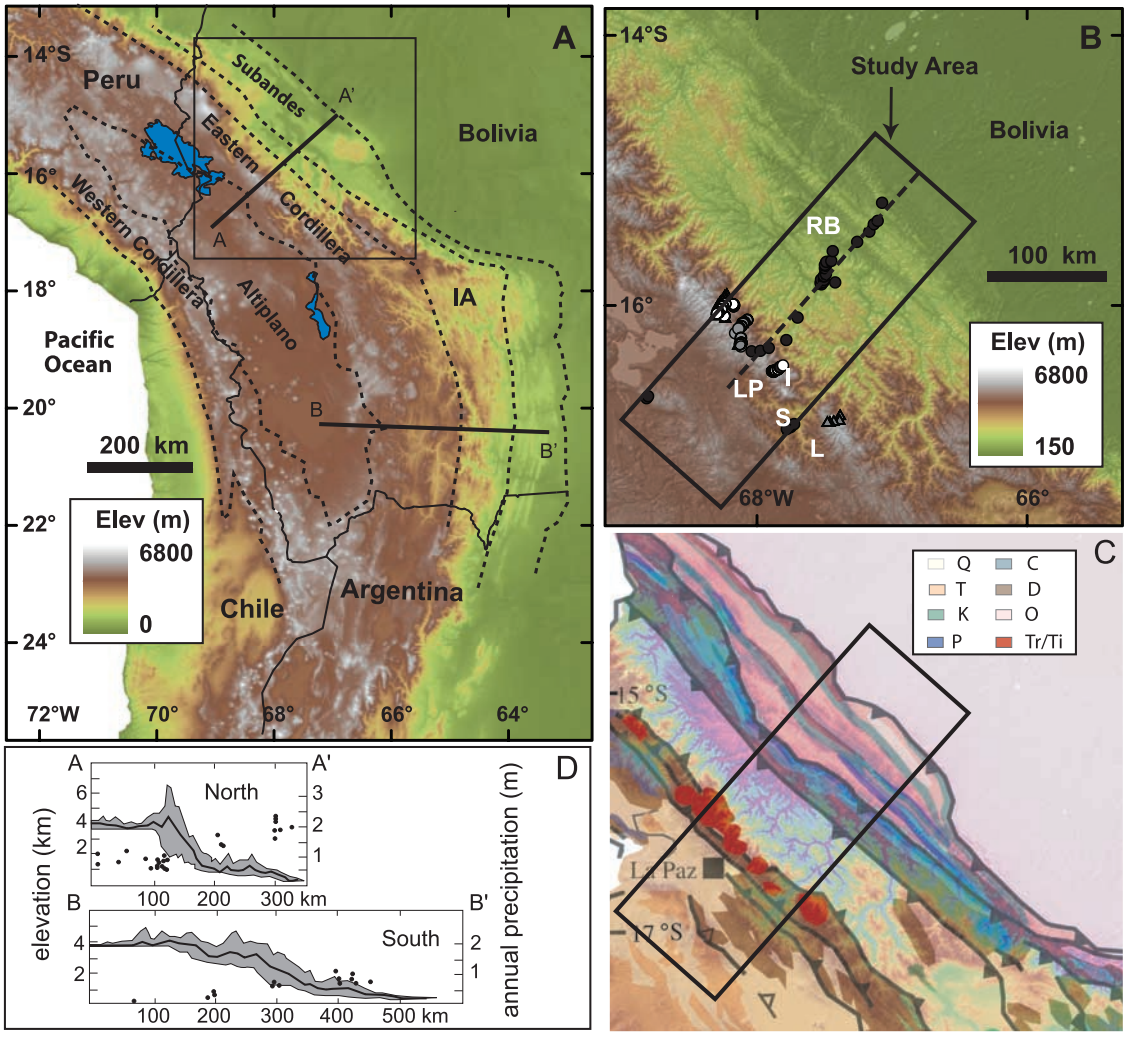

Figure 1. Morphology of the central Andean fold-thrust belt and Andean Plateau, Bolivia. (a) Digital topography (USGS GTOPO30 1 km) highlighting major physiographic divisions (dashed lines) and country boundaries (solid lines). Note the differences in size and topographic expression of the SA between northern and southern Bolivia. IA, Interandean zone. (b) High-resolution (SRTM 90 m) digital topography of the northern plateau margin. Location indicated by box in Figure 1a. The higher-resolution topography displays the morphological expression of the SA that gets muted out at the lower resolution in the westernmost margin of the IA. Two extensive canyon systems breach the Eastern Cordillera axis and drain the Altiplano. The southern system is occupied by Rio La Paz (LP), Rio Luribay (L), and Rio Sapahaqui (S). The southern drainage system has uniquely exposed the structural transition between the Altiplano and the Eastern Cordillera. I, Illimani. Rios La Paz, Luribay, and Sapahaqui all drain into the Rio Beni (RB) drainage system. Thermochronometer samples are compiled from this study and *Barnes et al.* [2006] (black circles), *Gillis et al.* [2006] (gray triangles), *Safran et al.* [2006] (white circles), and *Benjamin et al.* [1987] (gray circles). Dashed line is the profile location in Figures 4a and 4b. (c) General geologic map of Bolivia (simplified from *Guarachi et al.* [2001]) overlain on SRTM DEM. Colored symbols for map are Quaternary (Q), Tertiary (T), Cretaceous (K), Permian (P), Carboniferous (C), Devonian (D), Ordovician (O), Triassic/Tertiary Intrusions (Tr/Ti). (d) Topography and precipitation profiles from *Horton* [1999]. Maximum, mean, and minimum topography is based on a 100-km-wide bin along each profile. Mean elevation is black line; maximum-minimum elevation is shaded to highlight the latitudinal relief contrast. Profile locations are indicated in Figure 1a. Projected mean annual precipitation measurements are represented by black dots.

Figure 2. Photo of the Rio La Paz and Rio Sapahaqui drainage systems incised into the Eastern Cordillera. The photo is taken in the Rio Sapahaqui drainage basin looking ENE at Illimani (labeled I in Figure 1).

structure [*Roeder*, 1988; *Roeder and Chamberlain*, 1995; *Sempere et al.*, 1990].

[9] Recent work by *Barnes et al.* [2006] presented 19 new AFT and zircon (U-Th)/He (ZHe) samples across the location of the cross section. They combined new and previously published samples to document spatial and temporal variations in erosion across the northern Bolivian thrust belt. *Barnes et al.* [2006] and *Gillis et al.* [2006] found two rapid stages of exhumation: (1) Eocene to late Oligocene (~40–25 Ma) initial rapid erosion of the plateau margin and (2) accelerated, distributed erosion across the entire thrust belt since the early to mid-Miocene (~15 Ma).

3. Methods

[10] Methods used in this study include geologic mapping at 1:100,000-scale, cross-section construction and balancing, and low-temperature thermochronology samples tied to the balanced cross section. Details of these different methods employed are outlined below.

3.1. Geologic Mapping

[11] Our new geologic map and cross section are built upon previous results from surrounding areas [*Servicio Geologico de Bolivia (GEOBOL)*, 1994a, 1994b, 1995a, 1995b, 1996; *Guarachi et al.*, 2001; *McQuarrie and DeCelles*, 2001]. We present new data along a NE-SW transect (15–17°S) from La Paz to Yucumo, a cross-strike distance of ~200 km (Foldout 1). Original maps were produced at a scale of 1:100,000 and then compiled on to 1:250,000-scale topographic maps in conjunction with existing (1:100,000, 1:250,000 and 1:1,000,000) geologic maps. The development of the Rio La Paz, Rio Luribay and Rio Sapahaqui drainages expose the structural transition between the Altiplano and the Eastern Cordillera, providing exposures unique to this part of the fold-thrust belt (Figures 1 and 2 and Foldout 1). The southwestern portion of our transect takes advantage of the excellent exposure through this region. The road from La Paz to Yucumo via Coroico and Caranavi transects the entire fold-thrust belt in the Beni drainage basin (Foldout 1). However, only 20 km of the 100-km-wide back thrust belt is exposed along this road. To take advantage of both the exposure offered by the Rio La Paz and the access to the rest of the thrust belt offered by the road, we have a transect break that corresponds to significant along-strike structures, allowing the cross section to be accurately projected from one segment to the other (Foldouts 1 and 2).

3.2. Fission Track Thermochronology

3.2.1. General Overview

[12] We present new fission track analyses sampled from Ordovician to Devonian bedrock exposed across the EC and IA zones at ~15–17°S which is dominated by fine-grained, marine metasiliciclastic rocks. These samples augment those of *Barnes et al.* [2006] and provide new constraints on the cooling history of both previously unsampled and sampled structures.

[13] Apatite and zircon fission track (AFT and ZFT) thermochronology are sensitive to rock cooling in the upper crust (~10 km depth) over temperatures ranging between ~90–250°C [e.g., *Reiners et al.*, 2005]. Fission tracks form from the spontaneous fission of ^{238}U, are only quantitatively retained above a closure temperature, and subsequently shorten (anneal) over a temperature range below the closure temperature, called the partial annealing zone (PAZ) [e.g., *Fitzgerald et al.*, 1995]. The closure temperature of typical apatite is ~110 ± 10°C and its PAZ spans from ~110 to 60°C, whereas the closure temperature for common zircon is ~240 ± 25°C [e.g., *Brandon et al.*, 1998].

[14] For sedimentary rocks, a sample cooling age, often reported as a pooled age, is determined by summing ("pooling") the daughter/parent ratio of ~20+ individual grains together [e.g., *Brandon et al.*, 1998]. A χ^2 test is applied to the distribution of single grain ages to determine its degree of variance within a sample [*Galbraith*, 1981; *Green*, 1981]. Concordant ($P(\chi^2) > 5\%$) samples pass the χ^2 test with low variance indicating the pooled age is geologically significant [*Brandon et al.*, 1998; *Galbraith*, 1981; *Green*, 1981]. Conversely, discordant ($P(\chi^2) < 5\%$) samples "fail" the χ^2 test with substantial age variance rendering the pooled age less meaningful [*Green*, 1981; *Tagami and O'Sullivan*, 2005].

[15] Sedimentary rocks often produce discordant ages because individual grains have multiple sources and variable compositions, the latter of which is known to influence the annealing behavior [*Green*, 1981; *Tagami and O'Sullivan*, 2005]. For discordant samples, it is important to identify the reset (younger than the sample deposition age) and unreset (older than deposition) components [e.g., *Brandon et al.*, 1998]. As a result, several methods have been developed to statistically deconvolve the significant component grain age populations and/or combine that with measured track length distributions and apatite composition proxy data (e.g., Dpar) to quantify permissible cooling histories with inverse thermal modeling

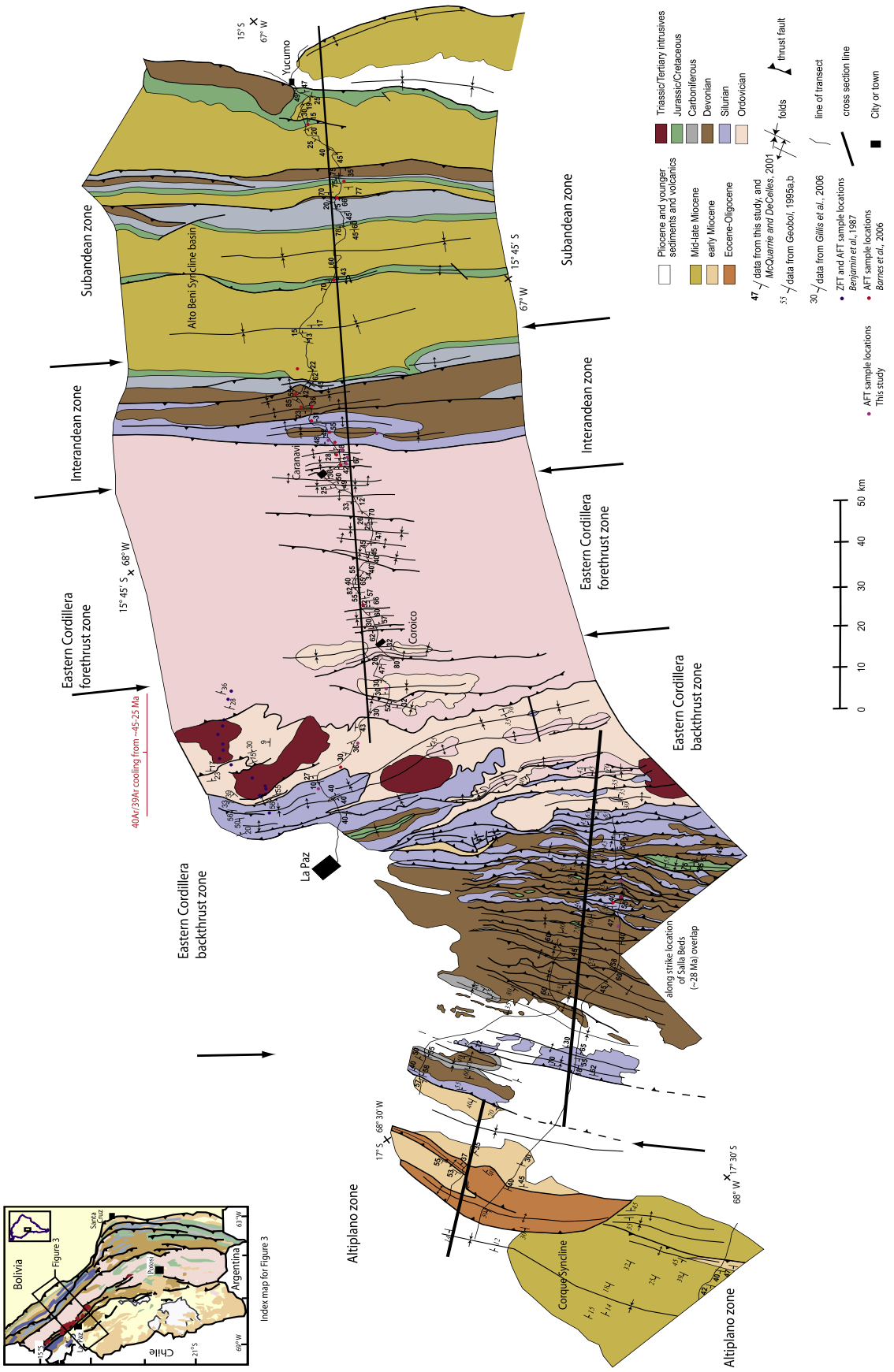

Foldout 1. Geologic map and thermochronometer samples through the Andean fold-thrust belt along the Rio Beni drainage system in northern Bolivia (17–15°S). The map is compiled from *Guarachi et al.* [2001], *GEOBOL* [1995a, 1995b, 1995c, 1994a, 1994b, 1996], and our own mapping.

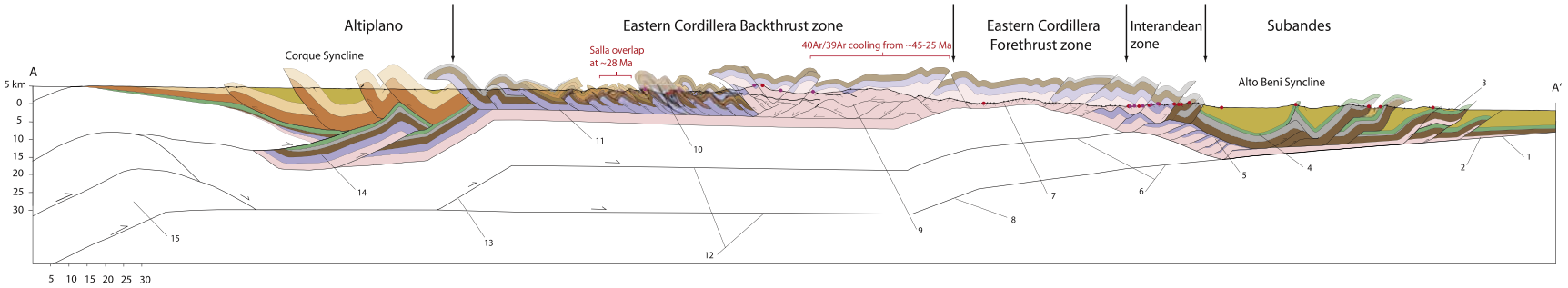

1. Thickness of foredeep and slope of basement determined from industry seismic reflection lines, gravity and well data [*Watts et al.*, 1995; *Baby et al.*, 1995; *Zubieta Rossetti et al.*, 1996].
2. Towards the northeast the thickness of Ordovician and Devonian rocks decrease, the Silurian disappears and the Carboniferous and Permian progressively wedge out [*Baby et al.,* 1995].
3. Map expression of broad fold NE of Yucumo suggests that Cretaceous and Devonian rocks are close to the surface below Tertiary rocks exposed at the surface. Dip of strata to the south suggests that this fold, and the postulated horse containing Ordovician through Cretaceous rocks, die out to the south.
4. Alto-Beni syncline contains 6.5-7 km of Tertiary sediments [*Baby et al.,* 1995].
5. Gradual increase of Silurian to explain thickness of Silurian in the IAZ and lack of Silurian strata in frontal structures in northern Bolivia [*Guarachi et al.*, 2001]. Horses of Ordovician and Silurian rocks balance the amount of shortening in Devonian and younger rocks in the SAZ.
6. Gradual increase in structural elevation from Alto Beni basin to Eastern Cordillera is explained by the alignment of 2 basement hanging wall cutoffs.
7. Deepest exposed portion of fold-thrust belt. Pervasively folded rocks suggest shortening amounts for this area could be underestimated by as much as 50% (30 km),
8. Footwall cut-off for SAZ basement thrust.
9. Gently undulating structural surface, with small fault offsets can be explained by underlying duplex in Ordovician rocks. Duplex in Ordovician rocks is needed to balance shortening in Silurian and younger rocks in the Backthrust zone.
10. The strata above the erosion surface represents shortening magnitudes in upper Devonian rocks. The excess Devonian were probably eroded as quickly as they were uplifted suggesting the structure, as drawn, may never have existed [*McQuarrie and DeCelles*, 2001].
11. Silurian age rocks exposed at the eastern and western edges of this zone of west verging thrusts suggest the decollement level is at the base of the Silurian Uncia Formation [*McQuarrie and DeCelles*, 2001].
12. Although basement thrusts are drawn as discrete faults, this does not preclude the development of shear zones associated with thrusting. Analogues with exposed, large offset basement thrusts suggest thrust-related fabrics are mostly concentrated in or near the fault zone at the base of the thrust sheet [*Hatcher and Hooper,* 1992].
13. Footwall ramp for upper basement thrust. Basement ramp is the preferred solution to explain the ~12 km stratigraphic offset between the Backthrust zone and Tertiary rocks in the Altiplano [*McQuarrie and DeCelles*, 2001].
14. This Paleozoic section may not be present. At Jesus de Machaca, 70 km to the NW, Cretaceous rocks overlie Upper Proterozoic to Lower Cambrian Sedimentary and volcanic rocks Chilla Complex [*Geobol*, 1997]
15. Magnitude of slip on "potential" basement horses is 66 km. In model, basement horses accommodate thickening of the western portion of the orogen associated with underthrusting of the Brazilian shield. Slip on thrusts is fed into the SAZ.

Mid-late Miocene	1-7 km	(1)
early Miocene	3-5 km	(5, 6)
Eocene-Oligocene	2-5 km	(5, 6)
Jurassic/Cretaceous	0-1 km	(1, 2)
Carboniferous	0-1.3 km	(1, 2)
Devonian	1.1-4.6 km	(1, 2, 3, 4)
Silurian	0-2.2 km	(1, 2, 3, 4)
Ordovician	0.5-6+ km	(1, 4)
Basement	12-15 km	(*)

(1) *Baby et al.*, 1995; (2) *Sempere*, 1995, (3) *Gonzalez et al.*, 1996, (4) *Suarez Soruco and Diaz Martinaz,* 1996, (5) *Horton et al.*, 2001, (6) *Horton et al.*, 2002,

(*) Basement thickness is based on magnitude needed to accommodate large stratigraphic offsets and fill space [*McQuarrie*, 2002; *Kley,* 1996]. Basement is assumed to detach at brittle ductile transition zone [*Hatcher and Hooper,* 1992; *Hatcher,* 2004].

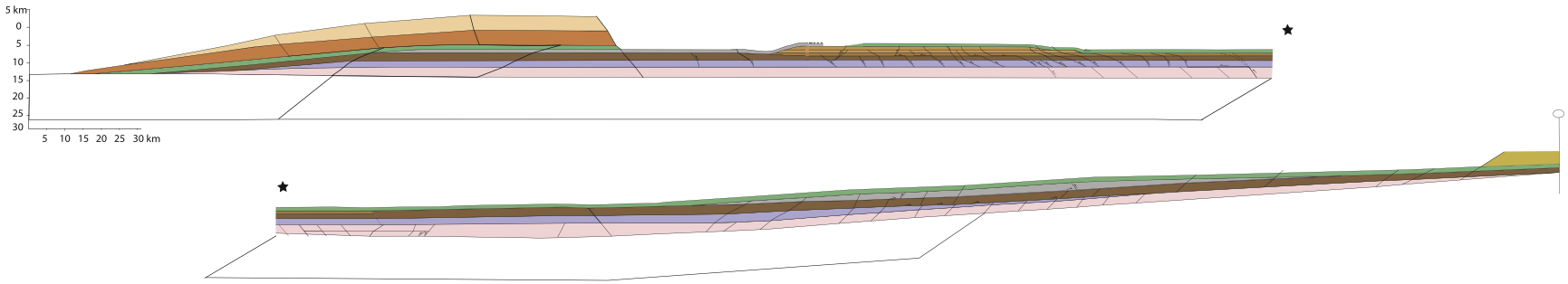

Foldout 2. Balanced and restored cross section through the Andean fold-thrust belt in northern Bolivia with apatite fission track samples from *Barnes et al.* [2006] (red circles) and new samples (purple circles) presented here.

[*Barnes et al.*, 2006; *Brandon et al.*, 1998; *Donelick*, 1993; *Ehlers et al.*, 2005; *Galbraith*, 2005; *Ketcham et al.*, 1999; *Ketcham*, 2005].

[16] The simplest application of cooling ages is to interpret the timing of cooling due to faulting, erosion, or magmatism [*Ehlers*, 2005]. In this study, we focus on documenting the timing of erosion across each zone, inferring that the topography needed for the initiation of rapid (defined as $>\sim$10°C/Ma) erosion-driven cooling through the closure temperature results from structurally generated relief [after, e.g., *Barnes et al.*, 2006].

3.2.2. Analytical and Modeling Procedures

[17] We used standard mineral separation techniques and the new laser ablation method for fission track analysis [*Donelick et al.*, 2005; *Hasebe et al.*, 2004] (see Appendix A for analytical procedure details). Following age analysis, age, and track length measured apatite grains were classified for annealing kinetics with the parameter Dpar, defined as the fission track etch pit diameter parallel to the crystal c axis at the polished grain surface [*Burtner et al.*, 1994]. We quantified the new sample thermal histories with inverse modeling of the AFT data using HeFTy [*Ehlers et al.*, 2005; *Ketcham*, 2005] and the multikinetic annealing model of *Ketcham et al.* [1999] (see Appendix B for details of the modeling methodology).

4. Results

4.1. Geologic Mapping

[18] The central Andean fold-thrust belt can be divided into major tectonostructural zones based on suites of structures with similar vergence, geometries and structural levels (Figure 1) [*Kley*, 1996; *McQuarrie*, 2002; *McQuarrie and DeCelles*, 2001]; the foreland, the Subandes (SA), the Interandean zone (IA), the Eastern Cordillera (EC), and the Altiplano. The sections 4.1.1–4.1.6 discuss the map patterns characteristic of each zone with increasing complexity westward from the foreland to the Altiplano and outline the constraints each area imparts to an orogen-scale cross section through the central Andean fold-thrust belt at 15–17°S (Foldouts 1 and 2).

4.1.1. Foreland

[19] The depth of the foreland basin in front of the northern Andean fold-thrust belt is defined through seismic, gravity and well data [*Baby et al.*, 1995; *Watts et al.*, 1995; *Zubieta Rossetti et al.*, 1996]. This region is a site of active deposition of synorogenic sediments [*Aalto et al.*, 2006] and has accumulated up to 5000 m of Tertiary synorogenic deposits [*Baby et al.*, 1995; *Watts et al.*, 1995]. Pre-Paleozoic basement is exposed on the eastern edge of the basin, $\sim$200 km to the east of the frontal thrust, and slopes 4° toward the orogen [*Baby et al.*, 1995; *Watts et al.*, 1995].

4.1.2. Subandes

[20] The Subandes are characterized by broad, large wavelength (10–20 km) synclinal basins separated by narrow zones ($\sim$1–5 km wide) of thrust-faulted anticlines. Seismic data across the Alto Beni syncline indicates that this piggyback basin contains very thick (6500–7000 m) Tertiary basin fill and is segmented into two subbasins by a narrow fault propagation anticline in Cretaceous age rocks (Foldout 1) [*Baby et al.*, 1995]. To the east of the Alto Beni basin are three thrust faults that carry Devonian through Tertiary age rocks in their hanging walls and exhibit stratigraphic separation of 5–10 km. Regional map patterns shown in Foldout 1 and on the 1:1,000,000-scale map [*Guarachi et al.*, 2001] suggest detachment horizons at the base of Ordovician, Devonian, and Cretaceous strata.

4.1.3. Interandean Zone

[21] The Interandean zone marks a rapid increase in structural elevation, or the elevation of rocks with respect to the undeformed foreland, from the axis of the Alto Beni syncline to the folded and faulted lower Paleozoic rocks exposed through this zone (Foldout 1). The smooth, but dramatic $\sim$12 km increase in structural elevation over a 20–30 km distance is unique to this region of the central Andes and is essentially double the observed structural step from the SA to the IA in the southern portion of the fold-thrust belt [*Kley*, 1996, 1999; *McQuarrie*, 2002]. Once gained, the structural elevation is consistently maintained across $\sim$80 km of the EC. The IA in the Rio Beni drainage basin consists of four faults spaced 3–10 km apart and folds with wavelengths of 3–5 km. The displacement magnitudes on individual faults range from 1 to 5 km, with stratigraphic separation of 0.5–3 km.

4.1.4. Eastern Cordillera

[22] In the eastern portion of the Eastern Cordillera, the structural level of the fold-thrust belt remains in lower Ordovician phyllites and slates for a length of $\sim$50 km. Folding is ubiquitous at several scales from wavelengths of tens of meters to 10 km. Most regional folds have a wavelength of $\sim$1 km. The deepest rocks exposed on the Rio Beni transect crop out in this region between Coroico and Caranavi and the metamorphic grade approaches upper greenschist facies (Foldout 1). Metamorphism in parts of the Bolivian Andes reaches as high as silliminite grade in the high peaks of the EC [*Gillis et al.*, 2006; *Safran et al.*, 2006]. However, these contact-metamorphosed, high-grade rocks surround Triassic plutons and may not represent the deepest rocks exhumed from the orogen.

[23] West of Coroico, the exposure level of rocks is at the contact between lower Ordovician phyllites and upper Ordovician quartzites (Foldout 1). For 30–40 km, the structural level is again more or less constant as a gently folded, undulating surface that is broken by a few low offset (0.5–2 km) faults. The amplitude of folding is $\sim$1–2 km with wavelengths of $\sim$10 km.

[24] The structures exposed in the Rio La Paz, Rio Luribay, and Rio Sapahaqui drainages southwest of La Paz (Figures 1 and 2 and Foldout 1) were described in detail by *McQuarrie and DeCelles* [2001]. Here we emphasize a few key characteristics for comparison with the structures to the east. This portion of the transect is composed of west verging folds and thrusts that place older on younger rocks. There is a slight east to west younging of exposed strata from predominantly Ordovician rocks in the east to upper Devonian rocks in the west. However, lower Silurian rocks exposed at the western edge of the back thrust belt suggest that the basal decollement climbs into and stays

at the base of the Silurian Uncia Formation for most of the back thrust belt [*McQuarrie and DeCelles*, 2001]. Closely spaced structures (wavelengths of 2–5 km) indicate the detachment is at a fairly shallow depth, with respect to the rocks at the surface, and is uniform.

4.1.5. Altiplano

[25] One of the largest structures in the fold-thrust belt is at the boundary between the Altiplano and EC. Here, a thrust fault juxtaposes Silurian rocks against Tertiary conglomerates. The stratigraphic separation between the Silurian rocks in the back thrust belt and the youngest Tertiary rocks preserved in the axis of the syncline defines a 12-km structural step (Foldout 1) [*McQuarrie*, 2002; *McQuarrie and DeCelles*, 2001]. The Tertiary conglomerates are part of a ~250-km-long syncline composed entirely of Tertiary sedimentary rocks that reach thicknesses of ~ 10–12 km [*Horton et al.*, 2002]. The thickness of Tertiary (12 km) and Paleozoic (~8 km) rocks provides a minimum depth to basement of 20 km under the Altiplano. The 60-km-wide, 12-km-thick Corque Syncline in the central Altiplano [*Horton et al.*, 2002; *Lamb and Hoke*, 1997] bifurcates into two synclines separated by a smaller thrust fault in the northern Altiplano [*GEOBOL*, 1996]. The ~12 km stratigraphic separation at the Altiplano-EC margin could be accounted for by a duplication of the Paleozoic section (doubling minimum shortening estimates) or a relatively abrupt change in the elevation of the basement [*McQuarrie and DeCelles*, 2001].

4.1.6. Summary

[26] Cross sections through the central Andean fold-thrust belt in the region must account for (1) observed changes in structural elevation, such as the rapid and smooth increase in structural elevation from the SA to the EC and the abrupt change in structural elevation from the EC to the Altiplano, (2) uniform structural elevation over the 170 km length of the EC, where only lower Ordovician rocks are exposed for 100 km in the east and structural elevation gradually decreases to expose Silurian through Devonian rocks at the surface in the west, and (3) the variety of wavelengths of deformation, particularly the narrow wavelengths in the back thrust belt and easternmost EC, as well as the more open, low-amplitude folds in the central part of the EC.

4.2. Balanced Cross Sections

[27] Balanced cross sections were developed as a tool to produce more accurate and thus more predictive geological cross sections in the frontal, nonmetamorphic portions of fold-thrust belts [*Bally et al.*, 1966; *Dahlstrom*, 1969]. As the technique developed and the utility of balanced cross sections in deciphering the kinematic history of a region became evident, the applicability of the technique has widened to include entire orogens [*Beach*, 1981; *Boyer and Elliott*, 1982; *Butler*, 1983; *DeCelles et al.*, 2001; *McQuarrie*, 2002; *Srivastava and Mitra*, 1994]. In these orogen-scale sections, basement rocks above the brittle-ductile transition zone are treated as "competent" rocks above a weak detachment and incorporated into a balanced section accordingly [*Hatcher*, 2004; *Woodward et al.*, 1989]. The test of the validity of any balanced cross section is that it is admissible and viable [*Dahlstrom*, 1969; *Elliott*, 1983]. Admissibility is defined as a match between the structures drawn on the section and the structures that can be seen in the region of interest [*Dahlstrom*, 1969; *Elliott*, 1983]. A viable section is a section that can be restored to an undeformed state, e.g., the material in the cross section must equal that in the restored section, such that a major assumption in section balancing is that there is little to no out of plane motion of material. The viability of a cross section rests on the assumption that if we truly understand how structures form, then we should be able to take them apart [*Elliott*, 1983; *Woodward et al.*, 1989]. This implies that a key and often overlooked "proof" that a section is balanced is an incrementally balanced or sequentially restored section. Through sequential restoration it is possible to test that slip on deeper structures is fed through linked fault systems to the slip on shallower structures and then eventually to the surface. So for viability, not only do the line lengths and area need to balance on a deformed and restored section, but fault slip must be conserved along the entire path of a thrust system [*Boyer and Elliott*, 1982; *DeCelles et al.*, 2001; *McQuarrie*, 2002; *Woodward et al.*, 1989].

[28] One of the classic problems in constructing a balanced cross section is "filling space" between a known detachment horizon at depth and the structural elevation of the sedimentary rocks exposed at the surface [*Woodward et al.*, 1989]. In fact, the age and thickness of the structurally bound stratigraphic package used to fill space in a balanced section may be the largest source of uncertainty in shortening estimates [*Kley*, 1996]. Thus, the better documented the stratigraphic succession involved in the deformation, the more tightly constrained are the shortening estimates. The Paleozoic strata of Bolivia are well known and the units involved in the fold-thrust belt and their documented thicknesses are annotated on Foldout 2. Knowing the original stratigraphic section and its local and regional variations is key because both magnitude and width of marked changes in structural elevations predict the size and location of deeper structures within a fold-thrust belt even where seismic data are absent.

[29] The central Andes are well suited for orogen-scale balanced cross sections because the rocks exposed at the surface are essentially the unmetamorphosed sedimentary cover from which the balanced cross section technique was defined. Although there are no data that directly constrain the geometry of deeper basement structure, the regional map patterns described in section 4.1 impart a large-scale geometric framework that must be accommodated by structures at depth [*McQuarrie*, 2002].

[30] The cross section presented here was balanced using the sinuous bed method (Foldout 2) [*Dahlstrom*, 1969]. Area balance was used to account for thickening of hinge zones and thinning of limbs as documented from structures in the field [*McQuarrie and Davis*, 2002]. The reasoning and justification behind detailed aspects of each section are annotated on the balanced cross section.

4.2.1. Subandes

[31] Bedding orientation and thicknesses exposed at the surface, documentation of regional detachment horizons, and the regional dip of the basement as indicated by seismic studies [*Baby et al.*, 1995; *Watts et al.*, 1995] were used to

constrain the geometry of structures in the Subandes. The stratigraphic throw on the SA faults (5–10 km) combined with dip data supporting ramps and flats, suggest that the thrusts have large, 13–17 km, displacements and regional flats are at the base of the Ordovician and Devonian as well as the top of the Cretaceous (Foldout 2). Ordovician strata exposed in the frontal most thrust of the SA ~100 km north of our section [*Baby et al.*, 1995] suggests that the basal thrust along the Beni transect may also carry Ordovician strata, although the throw on the frontal most faults in our study area is not great enough to expose Ordovician age rocks at the surface, and the thickness of the Ordovician may be thin. SA structures west of the three frontal structures are too narrow to include a westward thickening package of Ordovician rocks (Foldout 2). Shortening on these structures (~38 km), needs to be balanced by equivalent shortening in Silurian and Ordovician strata along a linked thrust system. We accomplish this by the duplexing of Ordovician rocks immediately east of the IA.

4.2.2. Interandean Zone

[32] The Interandean zone, as defined by *Kley* [1996], represents a zone of thin-skinned folding and thrusting that has been elevated with respect to equivalent strata to the east. To account for that elevation, we propose displacement on a basement thrust sheet that is active concurrently with the SA. The displacement of this basement thrust is equal to displacement on structures in Ordovician through Tertiary rocks to the east [*Kley*, 1996; *McQuarrie*, 2002]. Along the Beni transect, the IA is a narrow zone that extends from the western limb of the Alto-Beni syncline and includes four thrust faulted anticline-syncline pairs that increase in structural elevation to the east (Foldouts 1 and 2). The monotonic increase in structural elevation from the axis of the Alto-Beni syncline to the lowermost Ordovician rocks in the EC is unique to this portion of the thrust belt and we interpret this smooth increase to the alignment of two basement–hanging wall ramps (Foldout 2).

4.2.3. Eastern Cordillera

[33] The Eastern Cordillera along the Beni transect can be divided into three portions of slightly different structural and topographic elevations. The easternmost portion exposes the deepest rocks in the fold-thrust belt, which occur at the lowest elevations within the EC. Lowermost Ordovician slates and phyllites are pervasively folded and maintain a consistent structural elevation for ~50 km east to west (Foldout 2). We interpret this zone as a local structural high due to the repetition of two basement thrusts. This region of repeated basement is located east of the footwall basement ramp for the SA and west of the hanging wall ramp for the upper basement thrust sheet (Foldout 2). The combination of basement ramps defines a broad basement-cored anticlinorium at the eastern limit of the EC. This structure is present throughout the fold-thrust belt from 15.5°S to 21°S [*Kley*, 1996; *McQuarrie*, 2002]. We interpret the pervasive folding of lower Ordovician slates and phyllites as resulting from its proximity to the orogen-scale decollement at the base of the Ordovician.

[34] The westernmost part of the EC is the central Andean back thrust belt [*McQuarrie and DeCelles*, 2001]. The stratigraphy exposed at the surface ranges from Ordovician rocks exposed on the eastern edge to upper Devonian rocks exposed in the west. The style of deformation within the back thrust belt includes fault propagation folds and imbricate fans with the amount of deformation generally decreasing to the west (Foldout 2). The lowermost Silurian Uncia Formation is identified as the main detachment horizon for this region because it is the oldest unit consistently exposed in the hanging wall of thrusts and is recognized as a regional detachment horizon throughout the entire fold-thrust belt [*McQuarrie*, 2002; *McQuarrie and DeCelles*, 2001]. West verging folds and thrusts that place older on younger rocks, east to west younging of exposed strata, and the identification of west verging roof thrusts [*McQuarrie and DeCelles*, 2001] all suggest deformation in the back thrust belt propagated from east to west. The large magnitudes of shortening accommodated in the back thrust zone on Silurian and younger strata, requires comparable magnitudes of shortening in Ordovician strata.

[35] The gently folded, undulating surface of upper Ordovician strata immediately to the east of the back thrust belt is interpreted to be the roof thrust of a duplex formed in Ordovician strata (Foldout 1). The structural elevation of upper Ordovician rocks exposed at the surface and the depth to basement determined from the regional detachment level of the back thrust belt creates a space, ~7–10 km thick, that is best explained by horses of a duplex within Ordovician strata. The duplexing of Ordovican strata beneath the roof thrust provides a means to gently fold and fault the overlying rocks in a manner that is consistent with map patterns (Foldouts 1 and 2). Filling this space with duplexed Ordovician rocks instead of basement (similar to Figure 3c) is necessary to balance the shortening in the Silurian and younger strata to the west. This geometry allows slip on the duplexes to be transferred to faults within the Silurian and younger strata in the back thrust belt to the west. It also suggests that the zone of westward verging deformation extends much farther east, almost to Coroico (Foldouts 1 and 2).

4.2.4. Altiplano

[36] The cross section proposed here shows the Altiplano deforming through four west vergent faults (Foldout 2). The two central faults, which bound the east and west sides of the Corque syncline, are interpreted to have the most offset. The ages of the Tertiary rocks involved in the faulting range from ~50 Ma to 5 Ma [*Horton et al.*, 2002; *Lamb and Hoke*, 1997]. The basal detachment for the thrust faults is a shale and gypsum horizon at the base of the Eocene-Oligocene Potoco Formation [*Horton et al.*, 2002]. The magnitude of shortening of Tertiary rocks exposed on the Altiplano needs to be balanced with the amount of shortening in basement through Mesozoic rocks underneath the Altiplano. The geometry of the structures shown underneath the Tertiary rocks are the simplest structures that can fill space under anticlines and accommodate the 40 km of shortening calculated from the Tertiary sedimentary rocks.

4.2.5. Basement Deformation

[37] Figure 3 shows three cross sections across the Bolivian Andes at varying latitudes, which at this scale, emphasize basement deformation. Changes in structural

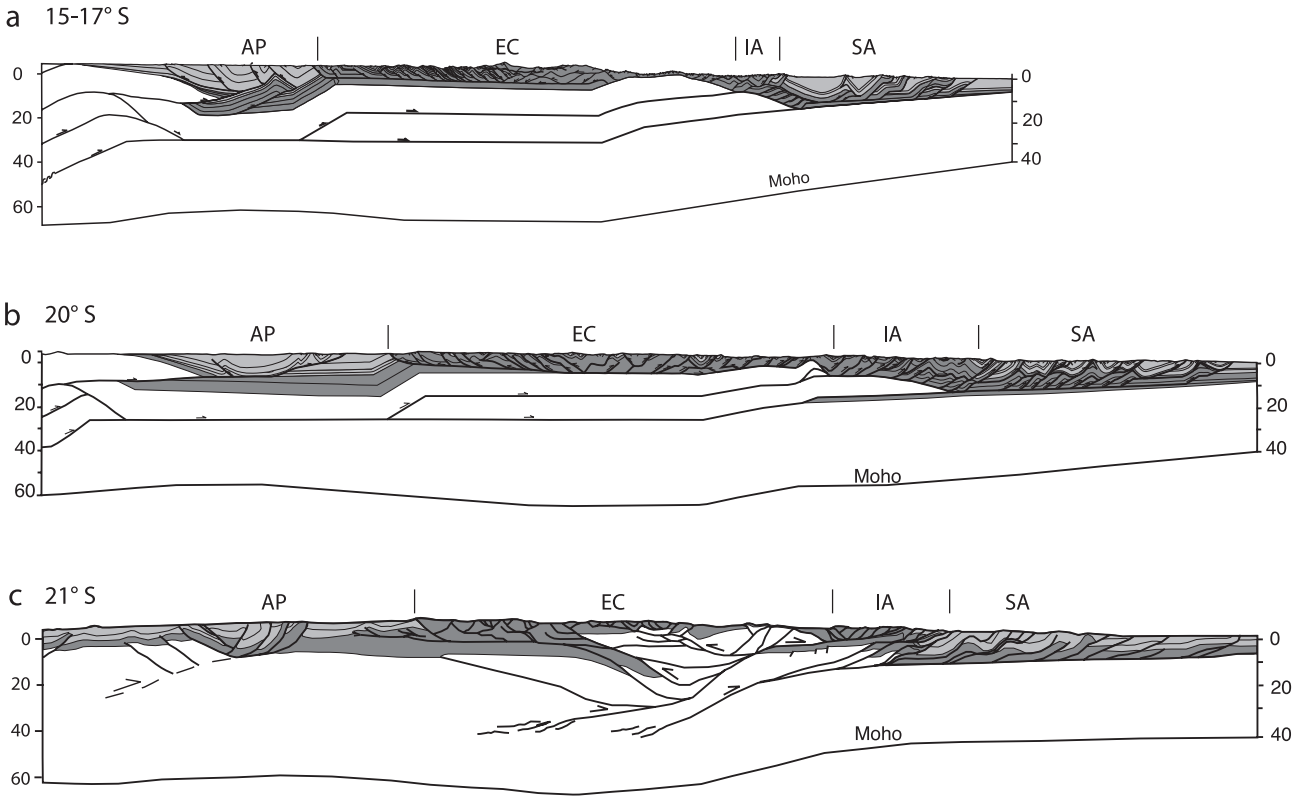

Figure 3. Mechanisms for basement accommodation of shortening in the Bolivian Andes illustrated by several crustal-scale cross sections. Sections are from (a) this study, (b) *McQuarrie* [2002], and (c) *Müller et al.* [2002] and *Elger et al.* [2005]. Moho for section A is from *Dorbath et al.* [1993], *Dorbath and Granet* [1996], and *Beck and Zandt* [2002]. Similarities in all three sections include relatively thin (10–15 km) basement thrust faults that accommodate 50+ km of displacement and account for abrupt changes in structural elevation adjacent to large regions with minimal change. Key difference in section C is the nature of basement deformation. Figure 3c shows multiple basement faults each different with regards to thickness of basement involved in thrusting, fault length, and fault displacement.

elevation within a fold-thrust belt do not reflect simple changes in decollement horizons. It is rather an effect of raising material as rocks are lifted up and over hanging wall and footwall ramps. These ramps can be in sedimentary rocks (creating a doubling of the sedimentary thickness) or in basement rocks [*McQuarrie*, 2002, Figure 5]. The space underneath the EC or IA cannot be accounted for by Paleozoic rocks, because the Subandean decollement projects deeper than the thickest Paleozoic strata in the EC or Altiplano [*McQuarrie*, 2002, Figure 5]. By using stacked basement thrust sheets to accommodate changes in structural elevation, the amount of shortening in the exposed Paleozoic and younger rocks equals the amount of shortening in the basement rocks assuring minimum shortening estimates. The basement geometry accounts for structural steps in both the hinterland (between the back thrust belt and the Altiplano) and foreland (between the SA and the EC) and provides a structurally high, flat decollement for the tight deformation of the EC to detach on (Foldouts 1 and 2).

[38] The exact nature of basement deformation (compare Figures 3a and 3b with Figure 3c) is not critically important. Figures 3a and 3b are separated by a north-south distance of ~600 km. In both locations, changes in structural elevation are compatible with ramps and flats of basement thrust sheets with thickness to length aspect ratios of ~1:15. About 100 km farther south (21°S), changes in structural elevation have also been explained by basement thrust sheets with similar aspect ratios (1:10) and similar detachment depths (~15 and ~25 km) [see *Müller et al.*, 2002, Figure 12]. However, in the southern model, the upper basement thrust sheet is also broken from the basal detachment to the sedimentary strata by several second-order east and west verging faults [*Müller et al.*, 2002] as well as several shallower decollement-like basement thrusts with thickness to length aspect ratios of 1:10 km. There is no a priori information about how the basement is deforming. However, the chosen geometry of basement deformation must explain several first-order geologic/geometric features seen throughout the fold-thrust belt in Bolivia such as the large-scale structural steps and the relatively flat nature of the decollement through the EC. Furthermore, interpreted basement structures must provide a kinematically viable way for deformation to accumulate through time, such that

the restored section can be sequentially deformed to produce the cross section. We chose the geometry of 2 stacked thrust sheets (Foldout 2 and Figure 3a) for the following reasons: (1) It is the simplest structure that is compatible with mapped geometrical constraints. (2) It is a kinematically viable solution that balances basement and upper crustal shortening [*McQuarrie et al.*, 2005]. (3) It provides a simple and direct test whether our proposed uplift induced exhumation (via basement thrust sheets) matches cooling ages in minerals.

4.2.6. Nonuniqueness in the Balanced Section

[39] A balanced cross section is a model that satisfies more reasonable constraints than a nonbalanced section and thus is more likely to be correct [*Woodward et al.*, 1989]. However, it is still nonunique, opening the possibility that different geometries and kinematics may be able to satisfy the same set of observations. Although the cross section is balanced, the most nonunique aspects of the cross section include (1) geometry of basement structure(s), (2) geometry of deformed strata at depth, and (3) thrust sequence. We discuss our interpretations with regard to these issues here.

4.2.6.1. Basement Structure Geometry

[40] With no basement exposed through the central Andes of Bolivia and a lack of reflection seismic data in the hinterland, basement geometries are not constrained by direct observation. However, as described by *McQuarrie* [2002], different basement geometries have predictable effects on surface geometries, kinematics, and mineral cooling ages. Other plausible basement geometries for the section presented here include duplexing of basement rocks or multiple basement faults as shown by *Müller et al.* [2002]. Duplexes impart a structural topography of domes and basins to the overlying stratigraphy due to the finite length and width (in map view) of horses that comprise the duplex [*Boyer and Elliott*, 1982; *Diegel*, 1986]. In contrast, the structural elevations (the level of exposed stratigraphy of the fold-thrust belt) that define the EC and IA are uniform [*McQuarrie*, 2002; *Kley*, 1999]. Structural highs and lows are concentrated around the eastern and western edges of the EC and are most easily attributed to hanging wall and footwall cutoffs of large basement thrust sheets [*McQuarrie*, 2002; *Kley*, 1999]. Multiple faults within the basement [i.e., *Müller et al.*, 2002] are another plausible basement geometry. We view the thrust sheet geometry as more plausible because a multiple basement fault interpretation entails a complicated fault geometry that is not reflected in the surface geology (similar to that described for duplexes) and it is difficult to reconcile with a viable kinematic scenario that will allow the various basement faults to feed slip into the sedimentary cover and accommodate the temporal and spatial variations in shortening.

4.2.6.2. Nonbasement Solutions

[41] Another possible explanation for the structural steps (i.e., pronounced changes in erosion level) mapped through the Bolivian Andes may be late (post 10 Ma) vertical uplift of the EC/IAZ due to removal of mantle lithosphere [*Garzione et al.*, 2006]. Support for this in the northern Andes are young (<15 Ma) cooling ages in the IA and EC [*Barnes et al.*, 2006; *Benjamin et al.*, 1987; *Gillis et al.*, 2006; *Safran et al.*, 2006] that may indicate increased exhumation due to recent, uniform, surface uplift of the EC and IA with respect to the Altiplano and Subandes. Arguments against the large structural steps being a result the proposed delamination are the following:

[42] 1. The map-scale extent of the structural high that defines the EC extends from southern Bolivia to southern Peru [*Kley*, 1999], while the broad region of young (<15 Ma) cooling ages are only north of 17°S [*Barnes et al.*, 2006, 2008; *Gillis et al.*, 2006; *Ege et al.*, 2007].

[43] 2. The westernmost boundary of the under thrust Brazilian shield has been imaged seismically as far west as the high peaks of the EC [*Beck and Zandt*, 2002; *Dorbath et al.*, 1993]. If the EC/IA boundary defines the eastern limit of rapidly removed lithosphere, the amount of postdelamination under thrusting of the Brazilian shield would require 120 km of shortening in the SA from ~10–0 Ma (we document 66 km).

[44] 3. The wavelength of the transition from low structural elevations (Altiplano and Subandes) to high structural elevation (EC) is ~20 km from the Altiplano to the EC and ~40 km from the EC to the Subandes. This implies that the structures accommodating these changes in structural elevation are in the upper 20–40 km of the lithosphere. Thus, if delamination is responsible for the mapped change from low to high structural elevation, it would need to be accompanied by high-angle faulting of the upper crust at the EC borders to accommodate the wavelength of deformation.

[45] 4. The data that indicate rapid, recent uplift are from the Altiplano [*Garzione et al.*, 2006], however the western boundary of the high structural elevation is the EC/Altiplano boundary [*McQuarrie and DeCelles*, 2001]. Delamination under both the EC and Altiplano cannot explain the ~12 km step between the Altiplano and the EC.

4.2.6.3. Deformed Strata at Depth

[46] Again, with the absence of reflection seismic data, the geometry of deformed strata at depth is also nonunique. However, deformed strata must fill space, balance (in length) the shortening documented on the surface and be kinematically viable with surface structures in overlying strata. Thus, for our purposes, the exact geometry is not as important as the requirements of length balance and kinematic compatibility. With known stratigraphic thickness, regional variations of strata, and shortening estimates, there is little ambiguity in shortening amounts accommodated by subsurface structures.

4.2.6.4. Thrust Sequence

[47] The balanced cross section and proposed sequential kinematic evolution were constructed under the assumption that faulting is forward propagating in the direction of transport whenever possible. Clearly out-of-sequence thrusts have been documented in several fold-thrust belts [*Morley*, 1988] as well as recognized in southern Bolivia [*Horton*, 1998; *Elger et al.*, 2005; *Ege et al.*, 2007] and northern Argentina [*Echavarria et al.*, 2003]. Within the EC of northern Bolivia, older units, deeper exposures and steeper faults in the east than in the west, as well as documented roof thrusts and duplexes require that most of the back thrust belt developed in sequence from east to west

[*McQuarrie and DeCelles*, 2001]. Out-of-sequence thrusts have been identified in southern Bolivia through AFT thermochronology and geochronology of synorogenic basin deposits [*Horton*, 1998; *Elger et al.*, 2005; *Ege et al.*, 2007]. Assumptions about thrust sequence are tested by a combination of thermochronology and kinematic reconstructions, described in sections 4.3.1–4.3.5.

4.3. Fission Track Thermochronology

4.3.1. Overview

[48] Figure 4 summaries all AFT data and associated thermal modeling results along the thrust belt transect at 15–17°S. Here we outline the results of the 10 new samples in the study and show several representative thermal histories in Figure 4d. The 10 new apatite fission track (AFT) results and one paired zircon fission track (ZFT) result were from bedrock exposures of Paleozoic quartzites in the EC and IA (Table 1). Pooled AFT ages range from 4 to 80 Ma with mean track lengths (MTLs) of ~11–14 μm and the one ZFT pooled age is 551 Ma (Table 1 and Figure 4b). The apatite Dpar values range from 0.74 to 2.2 μm with most values between 1 and 1.75 μm suggesting fast annealing calcian-fluorapatite compositions (Table 1) [*Donelick et al.*, 2005]. Four of the 10 AFT pooled ages passed the χ^2 test and the ZFT pooled age failed it. All 10 AFT pooled ages are reset (younger than deposition) and all samples possess $\leq$15% unreset individual grain ages suggesting the recorded cooling is Andean in age. The LA-ICPMS approach does not allow us to use the same statistical method of binomial peak fitting to resolve the component ages used by *Barnes et al.* [2006]. Furthermore, there is no straightforward delineation of kinetic populations because none of these samples show a correlation between Dpar and grain age or track length. As a result, we followed a conservative approach to interpreting the cooling history of all samples by modeling the thermal history from grain age and track length inversion [*Ketcham*, 2005]. We assumed one kinetic population and the only thermal constraint we placed on the inversion of sample cooling is that it must have been buried and heated sometime after deposition and then cooled through an AFT-sensitive temperature range of 50–180°C sometime (1) within $\pm 2\sigma$ of the pooled age for concordant samples or (2) between deposition and 1 Ma for discordant samples (see Appendix A for details). This approach tests the full range of sample cooling histories permitted by all of the measured grain ages and track lengths. Here we detail the results from west to east, which generally record Eocene to recent exhumation. The presentation of results from west to east allows for direct comparison with other Bolivia thermochronology studies [*Ege et al.*, 2003, 2007; *Barnes et al.*, 2006; *Scheuber et al.*, 2006].

4.3.2. Altiplano

[49] Two Altiplano AFT samples have been analyzed proximal to our study region ~85 km west of La Paz (Figure 1b) [*Barnes et al.*, 2006]. Collectively, they showed accelerated cooling from ~2–18 Ma.

4.3.3. Eastern Cordillera

[50] We report five new AFT ages, one with a paired ZFT age, from five thrust sheets in the EC (Figure 4). The first two samples (EC0-1 and EC2-1) are from the back thrust zone along the Rio La Paz and the remainder from the forethrust zone between La Paz and Coroico (Foldout 1). Sample EC0-1 has a discordant pooled age of 4.44 ± 0.98 (2σ) Ma with shortened tracks (MTL = 11.32 μm). No acceptable inversion model fits could be achieved for this sample. We interpret this sample as recording Pliocene cooling because (1) most grains (24 of 39) have <5 Ma ages and (2) it is consistent with results from three nearby samples (Figure 4b). Discordant sample EC2-1 has a pooled age of 49.8 ± 4.2 Ma, shortened tracks (MTL = 11.02 μm), and model results show rapid cooling from PAZ temperatures of ~75°C initiating 2–5 Ma (Figure 4b). Sample EC2-1 also has a discordant ZFT pooled age of 551 ± 50 Ma which is unreset relative to the age of deposition and hence considered detrital [*Brandon et al.*, 1998]. Concordant samples EC2-2 and EC3-1 have pooled ages of 8.3 ± 3.3 and 12.6 ± 4.6 Ma with long MTLs of >14 μm. Model results show rapid cooling initiated at $\geq$~110°C from 11 to 14 Ma and 16–20 Ma, respectively (Figures 4b and 4d). Sample EC3-2 has a discordant pooled age of 42.1 ± 16.8 Ma with reduced tracks (MTL = 12.43 μm). Model results suggest rapid cooling initiated from $\geq$~85°C between 30 and 50 Ma.

[51] In summary, integration of previous published AFT data with those presented here (Figure 4b) suggest (1) the EC experienced rapid cooling starting in both the mid-late Eocene (25–40 Ma) and mid-late Miocene to present (~0–15 Ma), (2) the EC back thrust zone exposed by the Rio La Paz drainage system has experienced local Plio-Quaternary (2–5 Ma) cooling probably due to recent fluvial incision [*Barnes et al.*, 2006], and (3) that there is significantly less exhumation in the back thrust zone of the Rio La Paz region

Figure 4. Topography, thermochronology, and structure across the central Andean fold-thrust belt at ~15–17°S. Figures 4a and 4b are modified from *Barnes et al.* [2006] (copyright (2006) with permission from Elsevier). (a) A 70-km-wide swath-averaged mean elevation profile from 90-m SRTM data with compiled sample locations projected onto the transect. Profile location is dashed line in Figure 1b. (b) Distribution of apatite fission track (AFT) ages across the thrust belt. Symbol legend and profile location are the same as in Figure 4a. Gray bars are the age range for the onset of the most recent rapid cooling constrained by modeling. Samples with <10 measured grain ages and/or track lengths are considered not robust results and excluded. (c) Balanced section with new sample locations highlighted. (d) Representative modeled thermal histories from the new AFT data showing acceptable (light gray), good (dark gray), and the best (line) cooling histories inverted from the AFT data. Boxes are fixed modeling constraints. C axis parallel track length (TL) distributions are shown for the data (histogram bars) and best fit (line) model. N, number of track lengths modeled. See Appendix A for additional modeling details.

as limited by an unreset ZFT age (551 Ma), whereas to the northeast there are reset ZFT and $^{40}Ar/^{39}Ar$ ages suggesting more significant exhumation of the forethrust zone (Figure 1b and Foldout 1) [*Benjamin et al.*, 1987; *Gillis et al.*, 2006].

4.3.4. Interandean Zone

[52] We report five new AFT ages from two thrust sheets in the IA (Table 1 and Figure 4). Discordant sample IA1-1 has a pooled age of 30.3 ± 11 Ma, moderate track lengths (MTL = 13.07 μm), and modeling shows rapid cooling

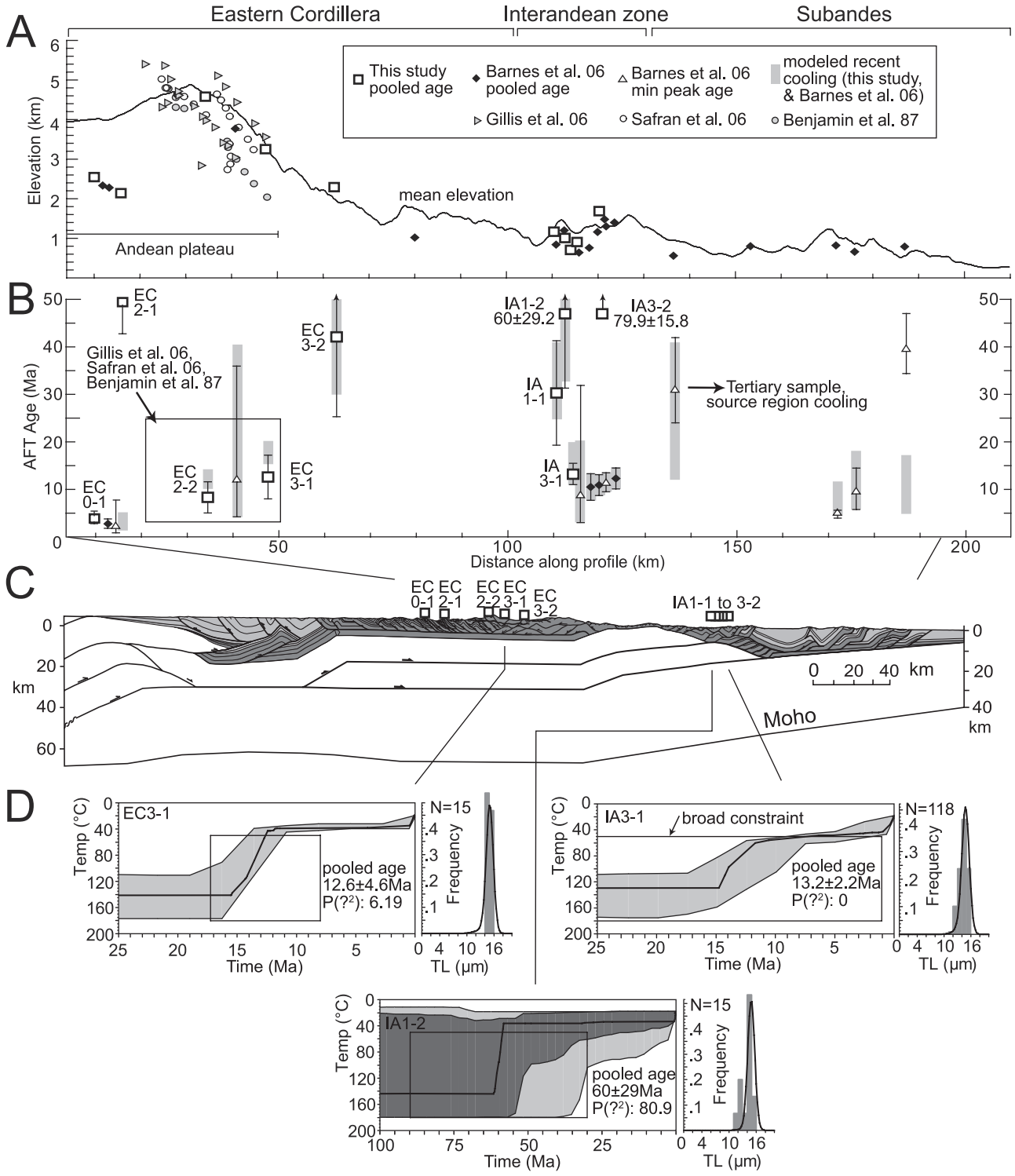

Figure 4

Table 1. Apatite Fission Track Analytical Data[a]

Sample	ID	Lat	Long	Elev, m	Fm Age	n	Dpar, μm	Dper, μm	N_s, tracks	Area, cm^2	$\Sigma(P\Omega)$, cm^2	$1\sigma\ \Sigma(P\Omega)$, cm^2	ξ_{MS}	$1\sigma\ \xi_{MS}$	P (χ^2), %	Pooled Age, Ma ± 2σ	MTL ± 1σ, μm (N_t, tracks)
									Eastern Cordillera								
05JBBL049	*EC0-1*	*−16.964*	*−67.796*	*2529*	*Dv*	*39*	*1.21*	*0.27*	*87*	*6.28E-04*	*1.62E-04*	*1.89E-06*	*16.6042*	*0.411*	*0.0*	***4.4*** ± *1.0*	*11.32 ± 1.85 (139)*
05JBBL050	*EC2-1*	*−16.877*	*−67.720*	*2148*	*Dv*	*40*	*1.32*	*0.27*	*934*	*1.06E-03*	*1.53E-04*	*1.55E-06*	*16.4345*	*0.408*	*0.0*	***49.8*** ± *4.2*	*11.02 ± 0.88 (168)*
725−16	EC2-2	−16.338	−68.041	4572	Ord	24	1.38	0.32	28	2.97E-04	2.90E-05	1.51E-06	17.2798	0.392	13.9	**8.3** ± **3.3**	14.05 ± 0.87 (26)
725−10	EC3-1	−16.312	−67.912	3246	Ord	14	1.51	0.30	35	2.13E-04	2.40E-05	1.63E-06	17.3361	0.393	6.2	**12.6** ± **4.6**	14.03 ± 0.69 (15)
724−18	*EC3-2*	*−16.254*	*−67.785*	*2286*	*Ord*	*14*	*1.60*	*0.33*	*29*	*2.21E-04*	*5.97E-06*	*4.34E-07*	*17.3759*	*0.394*	*0.0*	***42.1*** ± *16.8*	*12.43 ± 1.59 (19)*
									Interandean Zone								
JB01-L4	*IA1-1*	*−15.831*	*−67.530*	*1160*	*Ord*	*26*	*1.40*	*0.31*	*33*	*6.20E-04*	*9.47E-06*	*4.78E-07*	*17.4322*	*0.395*	*0.0*	***30.3*** ± *11*	*13.07 ± 1.24 (14)*
723−13	IA1-2	−15.824	−67.508	875	Ord	11	1.48	0.35	20	1.41E-04	2.90E-06	2.69E-07	17.4843	0.396	80.9	**60.0** ± **29.2**	12.62 ± 1.69 (15)
JB01-M2[b]	IA2-1	−15.807	−67.505	700	Ord	3	1.31	0.33	20	3.01E-05	5.52E-06	5.95E-07	17.5035	0.397	51.4	**31.7** ± **15.8**	12.55 ± 1.95 (5)
JB01-M5	*IA3-1*	*−15.778*	*−67.505*	*1023*	*Sil*	*36*	*1.53*	*0.32*	*216*	*7.33E-04*	*1.43E-04*	*6.51E-06*	*17.5625*	*0.398*	*0.0*	***13.2*** ± *2.2*	*12.95 ± 1.65 (118)*
JB01-M6	*IA3-2*	*−15.827*	*−67.423*	*1680*	*Dv*	*10*	*1.42*	*0.33*	*252*	*1.53E-04*	*2.76E-05*	*2.03E-06*	*17.6339*	*0.400*	*0.0*	***79.9*** ± *15.8*	*12.55 ± 1.76 (23)*
									Zircon								
05JBBL050	*EC2-1*	*−16.877*	*−67.720*	*2148*	*Dv*	*20*	*ND*	*ND*	*4194*	*1.27E-04*	*2.07E-05*	*3.50E-07*	*5.6694*	*0.2184*	*0*	551 ± 50	*ND (ND)*

[a]IA, Interandean zone; EC, Eastern Cordillera; Lat, south latitude (WGS84); Long, west longitude (WGS84); Elev, elevation; Fm Age, formation age; Ord, Ordovician; Sil, Silurian; Dv, Devonian; n, number of grains measured; Dpar, the mean maximum diameter of fission track etch figures parallel to the c axis; Dper, the mean maximum diameter of fission track etch figures perpendicular to the c axis; N_s, number of spontaneous tracks (tracks) counted; area, grain area analyzed; $\Sigma(P\Omega)$, area weighted $^{238}U/^{43}Ca$ (apatite) or $^{238}U/^{29}Si$ (zircon), summed over n grains in a sample; σ, standard deviation; ξ_{MS}, mass spectrometer zeta calibration factor; P(χ^2), percent probability of greater chi-square; MTL, mean track length; N_t, number of track lengths measured; ND, no data. Sample IDs are intended for easy integration with those previously published by the authors, e.g., IDs increase eastward; EC0-1 is west of EC1 from *Barnes et al.* [2006], EC2-1 and EC2-2 are located between samples EC2 and EC3 of *Barnes et al.* [2006], etc. Italics indicates samples that are discordant (P(χ^2) <5%. Bold values are referred to throughout the text.

[b]Less than 10 measured grain ages and track lengths.

started from ≥90°C 25–42 Ma (Figure 4b) with good fits constraining initiation between 30 and 38 Ma. Sample IA1-2 has a concordant pooled age of 60.0 ± 29.2 Ma with reduced tracks (MTL = 12.62 μm). Modeling shows cooling must have begun by ~30 Ma from ≥~85°C with good fits showing cooling by ~50 Ma (Figure 4d). Interestingly, the pooled age is dominated by 3 old grains (2 grains = 65–78 Ma, 1 = 658 Ma; 8 = <14 Ma). We tentatively interpret this sample to have cooled from PAZ temperatures by ~30+ Ma. Sample IA2-1 has a concordant pooled age of 31.7 ± 15.8 Ma with short tracks (MTL = 12.55 μm), but low grain/track yield (Table 1; excluded from Figure 4b). Modeling suggests acceptable cooling initiated from ≥~85°C by 19 Ma, with good fits suggesting even earlier, by 30 Ma. This result is consistent with two neighboring samples (pooled ages = 31 and 42 Ma both with <10 grains dated) [*Barnes et al.*, 2006]. Sample IA3-1 has a discordant pooled age of 13.2 ± 2.2 Ma with reduced track lengths (MTL = 12.95 μm). Modeling shows rapid cooling started ~14–18 Ma (Figure 4d). Finally, sample IA3-2 has a discordant pooled age of 79.9 ± 15.8 Ma with shortened tracks (MTL = 12.55 μm). Modeling suggests old cooling from ≥~80°C by ~55 Ma.

[53] In summary, integration of previous IA samples with those presented here (Figure 4b) suggests that the IA experienced two phases of cooling: (1) an early phase that started in the late Oligocene at the latest (by ~25 Ma) recorded by two robust samples (IA1-1 and IA1-2; Figure 4b) that are also consistent with several adjacent poorer quality samples (<10 grains dated) and (2) a later phase starting in the middle Miocene (~15 Ma) recorded by numerous robust samples derived mostly from the Devonian rocks exposed on the eastern half of the zone (Figure 4b). Substantiation of the earlier cooling phase is a new contribution of the AFT data presented in this study.

4.3.5. Subandes

[54] Five SA AFT samples from along our thrust belt transect have been analyzed previously [*Barnes et al.*, 2006]. The following is a brief summary of their cooling history from west to east (Figures 1b and 4). The westernmost sample cooled from ~100°C ~11–40 Ma which was interpreted to be a detrital signal and indicative of its source region cooling because it was sampled from Tertiary sandstone and had a discordant and old pooled and component ages. The next sample was very low quality with a poorly resolved cooling history. The three easternmost samples had discordant pooled ages (6.6, 51.5, and 91.4 Ma) with modeling of the reset components collectively constraining rapid cooling from PAZ or greater temperatures (≥~80°C) between 4 and 19 Ma.

5. Interpreted Tectonic and Exhumation History

[55] In this section we use the results from geologic mapping, balanced cross section generation, and mineral cooling ages to interpret the deformation and erosion history of the northern Bolivian fold-thrust belt. *Barnes et al.* [2006] and *Gillis et al.* [2006] document that thermochronometer cooling ages from the northern Bolivian thrust belt record cooling associated with erosional exhumation (as opposed to magmatism or tectonic exhumation via normal faulting). The simplest explanation for the mechanism behind the erosion responsible for sample cooling is that activation of structures in the sampled region generated topographic relief which lead to enhanced orographic precipitation and erosion. In this study, we make the assumption that the suite of new and compiled thermochronology samples from the Rio Beni region were erosionally exhumed and the earliest constrained rapid cooling provides an approximate timing for the initiation of deformation in a given zone. This approach allows a first-order interpretation of the kinematic history of the region, and provides valuable age constraints on forward modeling the sequential deformation of the section.

5.1. Shortening Magnitude

[56] The length of the cross section presented in this study is 414 km. The restored length of the cross section is 690 km indicating total amount of shortening for the entire section is 276 km or 40%. The EC accommodates the highest magnitudes of shortening, 123 km or 55%. The 123 km of shortening in the Eastern Cordillera is 44% of the total shortening within the fold-thrust belt at this latitude. The IA has shortened 48 km or 30%. This is only 17% of total shortening in the fold-thrust belt. Total shortening in the SA is 66 km. This is 40% shortening of the SA, but only represents 24% of total shortening of the fold-thrust belt. The Altiplano has shortened 40 km, which is 15% of the total shortening. The magnitude of total shortening associated with this section is 24–50 km less than sections farther to the south (17–18°S and 20°S) [*McQuarrie*, 2002], but the total percent shortening (the ratio of shortening to original length) is approximately the same at 37–40%.

5.2. Sequential Deformation

[57] A proposed sequential kinematic evolution for the Andean fold-thrust belt in northern Bolivia is presented in Figure 5 (see also Animation 1).[1] The evolution is based entirely on the geometric constraints discussed in sections 4.1 and 4.2 and shown in Foldout 2 and was initially created in 2DMove (Midland Valley) without data that constrain timing of deformation. 2DMove is a cross section restoration program that allows users to sequentially undeform a cross section or forward model a restored section. We forward modeled our restored cross section by inputting a fault system and a magnitude of displacement on that fault system. Motion on faults was accommodated by fault parallel flow of material. Fault parallel flow matches the first-order features of the fold-thrust belt, but does not match details such as the geometry of the fault propagation folds through the Eastern Cordillera [*McQuarrie and Davis*, 2002]. The sequential cross sections were constructed under the assumption that faulting is forward propagating in the

[1] Animations are available in the HTML.

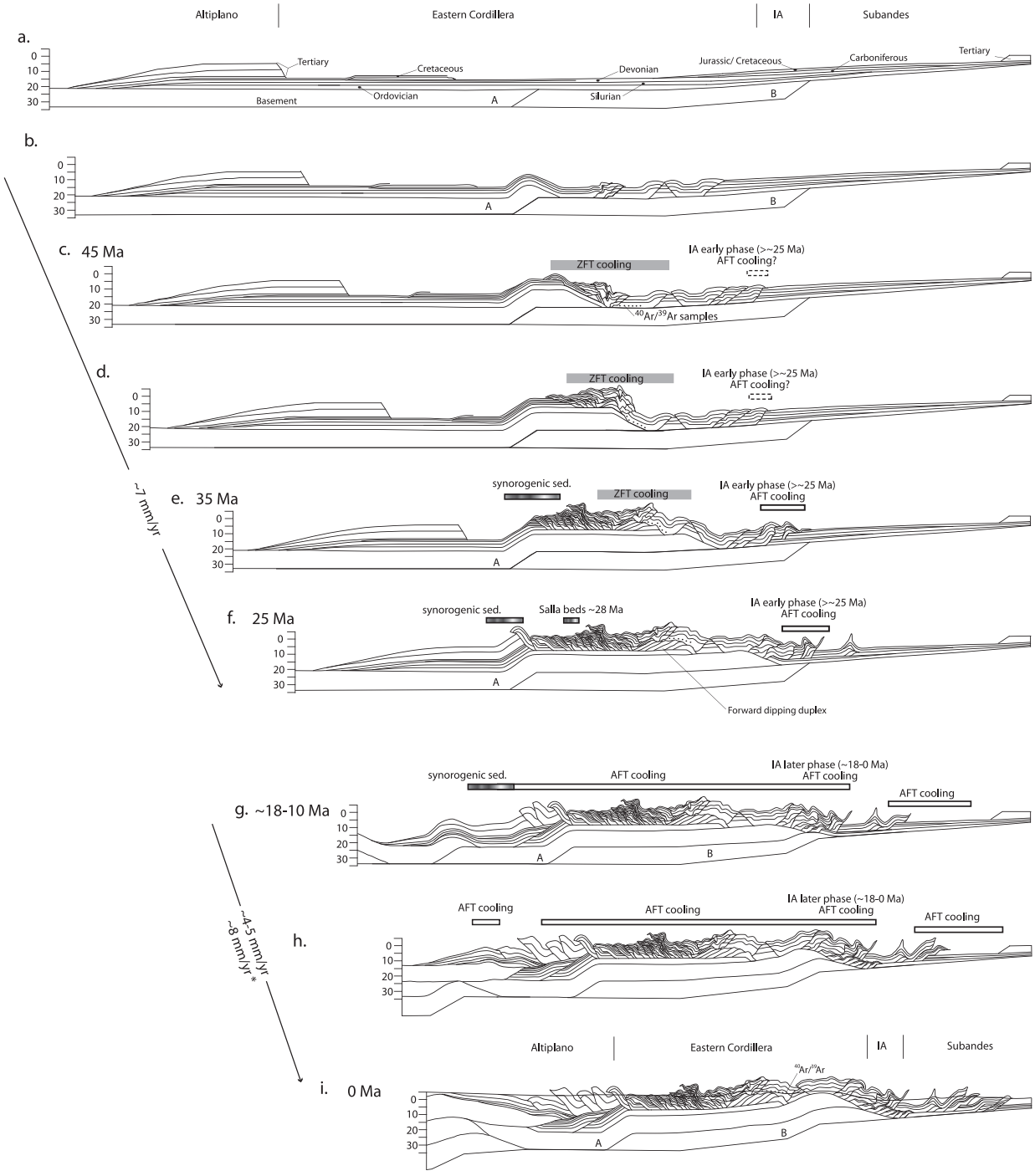

Figure 5. Kinematic evolution diagram showing the structural development of the Andean fold-thrust belt in northern Bolivia. The restored section (Foldout 2) is sequentially deformed in nine steps. Initial deformation was accomplished using purely geometrical and kinematic constraints. Ages along the left side of diagram and cooling bars above the sections are based on $^{40}Ar/^{39}Ar$, ZFT, and AFT thermochronology and local $^{40}Ar/^{39}Ar$ geochronology [e.g., *Gillis et al.*, 2006, *Barnes et al.*, 2006]. See Table 2. A and B refer to the first (upper) and second (lower) basement thrust sheets; see text for explanation and Animation 1 for sequential deveolpment.

direction of transport whenever possible. The goals behind this exercise are to (1) demonstrate that the basement geometry shown in the cross sections is kinematically viable in both magnitude and geometry of shortening and (2) create a sequential scenario for the fold-thrust belt that can be tested and constrained by thermochronology and the sedimentary record. The sequential deformation history presented here is broadly similar to previously presented histories for the Andean fold-thrust belt which incorporate the eastward propagation of basement thrust faults as the first-order control on cooling ages and the location and evolution of sedimentary basins [*Horton*, 2005; *McQuarrie*, 2002; *McQuarrie et al.*, 2005]. However, the details, such as how slip is transferred from the basement thrust to active faults in the sedimentary cover, the width and kinematics of the west verging back thrust zone, as well as the geometry of structures in the Paleozoic rocks, are specific to northern Bolivia.

[58] Shortening in the Ordovician and younger cover rocks accompanies emplacement of two basement thrust sheets at depth. In the first five time slices, emplacement of basement thrust sheet A in the west feeds slip into both east and west verging structures in the EC and IA. In the remaining three slices the now structurally lower basement sheet B feeds slip into the SA. The thrust sequence starts with initiation of deformation in the Eastern Cordillera (Figure 5b). We propose that deformation was transferred to the EC via the eastward propagation of the fold-thrust belt along the brittle-ductile transition ($\sim$15–20 km) and the extension of the basal detachment $\sim$300 km to the east. As the basal detachment propagated over a basement ramp, slip was fed eastward into a series of mostly east verging thrust faults in the sedimentary cover (Figure 5b).

[59] The next four time slices illustrate the development of the westward verging back thrust zone (Figures 5c–5f). The westward progression of fault propagation folds and associated thrusts in the Silurian and younger rocks is balanced by growth of a west dipping duplex in Ordovician rocks to the east. The eastward propagating basement thrust sheet (A) and growth of the duplex in Ordovician rocks structurally elevates 40 km of the EC deformed during the period shown in Figures 5b–5e. The eastward motion on the basement thrust fault (179 km) is mostly accommodated by 123 km of shortening in the EC and the development of the back thrust belt [*McQuarrie and DeCelles*, 2001]. In this interpretation, slip is fed first into east and west verging faults of the EC, then into the IA and the westernmost anticlines in the SA.

[60] Figures 5g–5i depict the coeval development of the Subandes, Altiplano, and the second basement thrust sheet (B). Displacement on faults in the SA (66 km) is balanced by displacement on the structurally lower basement thrust sheet, B. Motion of this thrust sheet elevates rocks in the eastern portion of the EC and rocks in the IA. Deformation documented in the Tertiary and younger rocks within the Altiplano must be accommodated at depth by shortening in the Paleozoic sequence and underlying basement. This coeval thrusting feeds $\sim$40 km of slip into the deforming Altiplano and 66 km of slip into the Subandean basement thrust and associated folding and faulting in the SA. Figure 5i illustrates the visual match between the forward modeled deformation in 2DMove and the original cross section shown in Foldout 2.

6. Discussion

6.1. Timing of Deformation

[61] By linking the cross section to thermochronometer cooling ages, the kinematic evolution presented in the previous section can be tested and the rates of deformation quantified (see also Animation 1). Figure 6 shows a simplified compilation of the Tertiary chronology and estimated exhumation magnitudes inferred from thermochronology across the thrust belt. Figure 6a shows the range of acceptable times for the onset of rapid cooling. These ranges were determined from both inverse modeling of the fission track data in this study and published data [*Barnes et al.*, 2006; *Benjamin et al.*, 1987; *Gillis et al.*, 2006]. Table 2 lists the shortening rates calculated from the chronologic constraints.

[62] The earliest cooling ages in the region come from high-elevation $^{40}Ar/^{39}Ar$ ages collected in the Eastern Cordillera that exhibit cooling histories extending from the Late Cretaceous through the Cenozoic [*Gillis et al.*, 2006]. Cooling paths show pronounced breaks in time-temperature space, which indicate an onset of rapid cooling at $\sim$40 Ma (Figures 5d and 6a). Topographically lower samples record more abbreviated histories with cooling initiating at 40–45 Ma and persisting to $\sim$26 Ma (Figures 5c–5f and 6a) [*Gillis et al.*, 2006]. The $^{40}Ar/^{39}Ar$ data also display a pronounced and systematic decrease in age from SW to NE. *Gillis et al.* [2006] argue that paired muscovite-biotite ages require that most samples originally resided within a narrow temperature window at 9–11.5 km depth and that structural uplift and subsequent exhumation propagated from SW to NE (Figures 5c–5f and 6b). Zircon fission track (ZFT) data collected nearby (Figure 6) also indicate that the onset of rapid cooling initiated at $\sim$40–45 Ma [*Benjamin et al.*, 1987; *Gillis et al.*, 2006].

[63] Incorporating these data with the sequential cross section restoration allows us to place absolute ages on the kinematic evolution presented in the previous section. For example, the $^{40}Ar/^{39}Ar$ data of *Gillis et al.* [2006] is shown in its restored place in the cross section (black dots in Figure 5c) at 45 Ma. The timing and magnitude of deformation in Figure 5b is unknown. However, the magnitude of deformation must be large enough to allow for $^{40}Ar/^{39}Ar$ and ZFT cooling at $\sim$45 Ma. [*Benjamin et al.*, 1987; *Gillis et al.*, 2006]. Between 45 Ma and 25 Ma, the samples are systematically structurally uplifted from west to east first by the eastward propagating basement thrust hanging wall ramp, and then uplifted as part of a westward verging roof thrust emplaced over a forward dipping duplex in Ordovician rocks (Figures 5c–5f). The growth of the duplex occurs synchronous with the development of the westward verging back thrust belt. The burial of the back thrust belt, by its own synorogenic sediments, constrains the cessation of thrusting. The age of these basin sediments range from 24.6 to 33.1 Ma [*GEOBOL*, 1997; *Gillis et al.*, 2006; *Kay et*

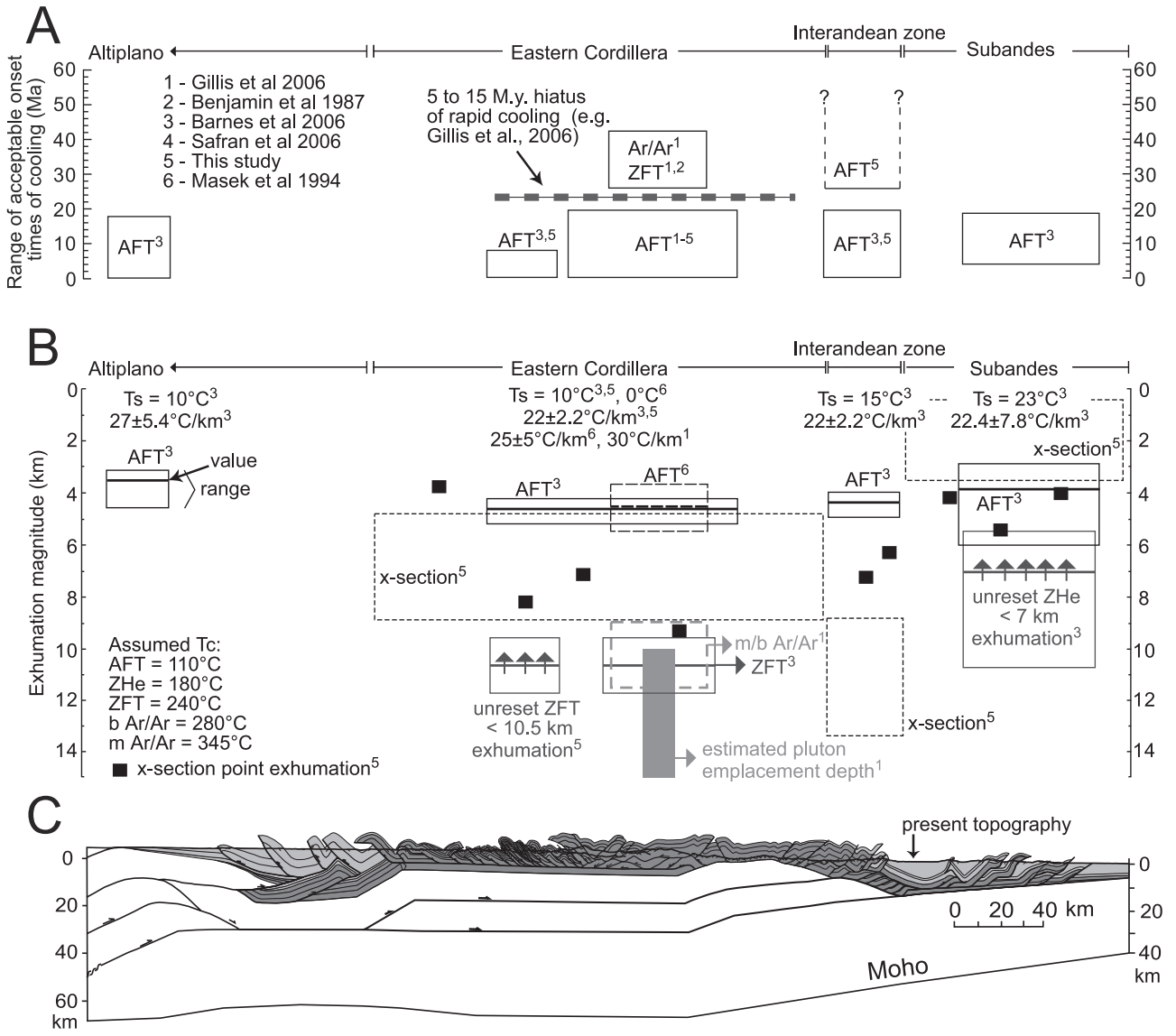

Figure 6. Thermochronologic constraints on the chronology and magnitudes of exhumation across the central Andean fold-thrust belt at ~15–17°S. (a) Distribution of recorded rapid cooling episodes inferred from various thermochronometer systems compiled from this study and others. See legend for appropriate references. Ar/Ar, muscovite and biotite $^{40}Ar/^{39}Ar$; ZFT, zircon fission track; AFT, apatite fission track. Note that the range of acceptable times for the onset of rapid cooling is shown. These ranges were compiled from the referenced studies and from the acceptable fits of inverse modeling of the fission track data in this study and *Barnes et al.* [2006]. (b) Estimated exhumation magnitudes. Assumed surface temperature (Ts) and geothermal gradients necessary to quantify these estimates are listed at the top of each region. Assumed closure temperatures (Tc) for the different thermochronometer systems are listed in the bottom left corner. Abbreviations and reference sources are the same as in Figure 6a; b, biotite; m, muscovite; ZHe, zircon (U-Th)/He. (c) Balanced section including the distribution and amount of material estimated to have been removed by erosion from above the present-day topographic surface.

al., 1998; *Lamb and Hoke*, 1997; *MacFadden et al.*, 1995; *McRae*, 1990; *Sempere et al.*, 1990; *Suarez and Diaz*, 1996]. Growth structures are observed within the Luribay Formation and the lower levels of the Salla Formation (25.5–29.4 Ma), but are not observed in the subhorizontal upper Salla Formation indicating that deformation ceased in this region by ~28 Ma (Figure 5f) [*Gillis et al.*, 2006]. Combining the sequential restoration, cooling ages and sedimentation record, 163 km of shortening accommodated in this portion of the fold-thrust belt had to have occurred between 45 and 25 Ma which translates into a rate of ~7 mm/a (Table 2). The pattern of older and higher

Table 2. Shortening Rates for the Andean Fold-Thrust Belt, Northern Bolivia

Location	Amount, km	Time Interval, Ma	Rate, mm/a
EC and IA	154–163	50–25	7.16
EC and IA	unknown	25–15	too low for cooling signal
SA	57–66	15–0	4.4[a]
SA	57–66	8	8.25[b]
Altiplano	40	15–0	2.67
Total	276	45–0	6.13

[a]Assuming oldest cooling ages represent initiation of deformation.
[b]Assuming that timing of SA deformation in northern Bolivia is the same as southernmost Bolivia [*Echavarria et al.*, 2003; *Garzione et al.*, 2006].

temperature cooling in the center of the EC, younger and shallower cooling in the western EC and IA, and synorogenic sediments that cap deformation in the westernmost EC by ~28 Ma is consistent with an eastward propagating basement thrust fault as the uplift impetus that initiates exhumation.

[64] AFT samples within the northern (15–17°S) EC of Bolivia have mostly provided young (~≤20 Ma; >40 ages total; Figure 4b) AFT cooling ages indicative of rapid cooling at ~15 Ma [*Barnes et al.*, 2006; *Benjamin et al.*, 1987; *Gillis et al.*, 2006; *Safran et al.*, 2006]. In addition, four samples collected in the La Paz drainage are as young as 2 Ma (Figure 4b). The combined $^{40}Ar/^{39}Ar$, ZFT and AFT data from the EC plutons of *Gillis et al.* [2006] indicate two pulses of rapid cooling, an initial period associated with deformation from ~45–25 Ma, followed by a second pulse unassociated with major deformation from ~15–11 Ma to present. Integration of mineral cooling ages, geometry of structural relationships, and crosscutting relationships of Tertiary basins indicate that deformation within the EC of Bolivia ceased by ~25 Ma and that the younger, ~15 Ma to present exhumation is unrelated to upper crustal shortening in the northern EC [*Barnes et al.*, 2006; *Gillis et al.*, 2006; *Horton*, 2005]. Recent fluvial incision into the Altiplano is interpreted to be responsible for Plio-Quaternary cooling recorded by four samples within the Rio La Paz, Luribay, and Sapahaqui drainages (Figures 1b and 4b) [*Barnes et al.*, 2006].

[65] AFT cooling ages in the IA range from 10.5 to 79.9 Ma (Figure 4b). Several samples of mixed quality, mostly along the western margin of the IA, have old (30+ Ma) pooled ages that record an early phase of cooling that initiated by at least ~25 Ma (Figures 4b and 6a). These early cooling ages agree with our proposed initial deformation within the IA (Figures 5c–5e). Of the remaining samples, many have ages between 10.7 and 14 Ma, with modeling results showing that the second phase of cooling initiated at ~15 Ma (Figure 4b) [*Barnes et al.*, 2006]. One low-grain-yield exception has a pooled age of 18.7 ± 9.6 Ma with no further model-constrained cooling [*Barnes et al.*, 2006]. Considering all the previous variations in cooling ages, the combined data suggest a second phase of rapid cooling between ~5–15 Ma at the 1σ uncertainty (Figure 4b) [*Barnes et al.*, 2006]. The young, cooling observed across this region is consistent with the eastward propagation of the Subandean basement thrust sheet over a ramp, which would have increased relief, and accelerated erosion across the topography spanning the width of the basement thrust (Figures 5g–5i) (see also Animation 1).

[66] Cooling histories of Devonian to Jurassic samples from the eastern SA indicate a partial resetting of AFT and no thermal resetting of zircon (U-Th)/He thermochronometers during the Tertiary (Figure 4b) [*Barnes et al.*, 2006]. Model-constrained cooling of individual thrust sheets in the SA suggest accelerated cooling initiated 19–4 Ma with the most rapid cooling between 12 and 5 Ma at the 1σ uncertainty [*Barnes et al.*, 2006]. Although the number of samples is small (three AFT cooling ages) each thrust in the SA has a significantly different age of cooling, different from the more uniform cooling of the Eastern Cordillera or IA. Accelerated cooling initiating between 19 and 4 Ma support deformation within the SA as old as ~15 Ma, providing a long-term shortening rate of 4.4 mm/a or a more rapid rate of 10–8 mm/a if deformation initiated as recently as 8 Ma (Table 2) as proposed for regions farther south [*Echavarria et al.*, 2003; *Elger et al.*, 2005], or inferred for northern Bolivia [*Garzione et al.*, 2006].

[67] Regional mapping, thermochronology, sedimentology of neotectonic strata and geochronology of volcanic rocks, suggest that deformation in the northern Altiplano occurred primarily between 11 and 5 Ma [*Lamb and Hoke*, 1997; *Barnes et al.*, 2006].

[68] If the initiation of cooling in each zone is a function of fault related uplift as suggested in this section, then the hiatus in cooling from ~25–15 or 8 Ma, suggests a pause or a dramatic deceleration in the rate of deformation and propagation of the Andean fold-thrust belt for 10–17 Ma.

6.2. Comparison of Exhumation Magnitude Estimates

[69] In this section, we compare denudation magnitudes estimated from the missing area above the balanced section and the thermochronometer data. By projecting stratigraphy and structure above the modern-day erosion surface, and including the predicted eroded section in the restored section, balanced cross sections can provide first-order spatial variations in the erosion magnitude [*Barnes and Pelletier*, 2006]. The balanced cross sections allow us to determine the minimum amount of exhumation above a given point (by measuring the removed material above the topographic line) as well as determine an area average of exhumed material for each zone. Estimates of cross-sectional area removed by erosion can be calculated by measuring the area of eroded strata above the present topography (Foldout 2 and Figure 6c). When younger strata is not shown (such as Cretaceous and younger rocks in the EC and IA), the area can be determined by the lengths of the youngest continuous contacts in conjunction with the average stratigraphic thickness of Cretaceous and Tertiary rocks. Dividing the estimate of area removed by erosion by the modern width of the thrust belt provides an average regional thickness of denudation. Clearly, assuming the missing rock areas are distributed uniformly is an oversimplification. This is especially evident by how localized exhumation can be above hanging wall cut offs such as in the SA or Altiplano (Foldout 2). The variation between average regional denu-

Table 3. Exhumation Estimates for Rio Beni Transect, Bolivia (15°–17°S)[a]

	Cross Section Estimate, km	Thermochron Estimate, km	Cross Section Estimate, mm/a	Thermochron Estimate, mm/a	Timescale
EC	4.8–8.8	9–11	0.11–0.19	0.2–0.24	from 45 Ma to 0
EC	–	5.5–7.5	–	0.18–0.375	from 45 to 25(15) Ma[b]
EC	–	3.5	–	0.23	from 15 Ma to 0
IA	8.8–13.4	4–5	0.59–0.89	0.27–0.33	from 15 Ma to 0
SA	0.39–3.4	3–5	0.03–0.23	0.2–0.33	from 15 Ma to 0
Total	3.75–6.71	5.3	0.08–0.15	0.12	from 45 Ma to 0

[a]Magnitudes of Tertiary sediments is 4 km in this portion of the SA. In all other parts of the FTB in the north and south it is 3 km. The 4 km in the northern SAZ section reflects much greater magnitudes of preserved Tertiary rocks there.
[b]The value in parentheses represents the minimum time of termination of deformation in this zone.

dation and predicted denudation at a given point on the cross section is illustrated in Figure 6. Even in light of significant variations, the exercise of determining regional denudation amounts is still informative because it allows a first-order comparison of the regional-scale spatial variations in exhumation to both locally derived thermochronometers and estimates of exhumation in other portions of the orogen [*Barnes and Pelletier*, 2006; *Barnes et al.*, 2008].

[70] Tertiary rocks preserved in intermontane basins throughout the EC are used to support the eastward migration of an early to middle Tertiary foreland basin that both predated and was synchronous with eastward propagating deformation [*Horton*, 2005]. Area and point estimates presented in here both include (upper range) and exclude (lower range) a 3-km-thick (in the EC) to 4-km-thick (in the SA) Tertiary section. The modern foreland basin in the northern Andes contains 4–5 km of Tertiary sedimentary rocks and piggyback basins within the SA preserve Tertiary thicknesses of 4–7 km [*Baby et al.*, 1995; *Roeder and Chamberlain*, 1995; *Watts et al.*, 1995]. Thickness of an early Tertiary section that may have overlain the EC and IA is unknown. For these parts of the fold-thrust belt we use a 3-km estimate that matches foreland basin estimates to the south [*Horton and DeCelles*, 1997]. Using this method, we estimate that 891–1610 km^2 of material was removed from the 183-km-wide EC, 194–295 km^2 of material was removed from the 22-km-wide IA, and 35–310 km^2 of material was removed from the 89-km-wide SA. Total magnitude of removed material is estimated to be 1120–2013 km^2 (Tables 3 and 4).

[71] Exhumation magnitudes constrained by thermochronology have already been estimated across the thrust belt by calculating the depth to average closure temperature from assumed and measured geothermal gradients and surface temperatures (Figure 6b) [*Benjamin et al.*, 1987; *Masek et al.*, 1994; *Barnes et al.*, 2006; *Gillis et al.*, 2006]. Table 3 is a comparison between denudation estimates derived from both the thermochronology and the cross section. The cross section estimate of material removed from the EC is 0.2–6 km less than that predicted by reset ZFT and ^{40}Ar/^{39}Ar ages. The range in exhumation estimates derived from the cross section is due to the inclusion (8.8 km of exhumation) or exclusion (4.8 km) of 3-km-thick foreland basin sediments that likely blanketed the region prior to deformation [*Horton*, 2005]. In addition, dividing the area of material removed by the length scale of the modern cross section averages the material over the entire length scale and assumes uniform exhumation across the entire zone, which in the case of the EC may not be appropriate. Even the simple change from lower Ordovician to Devonian rocks exposed at the surface (Foldout 1) indicates there has been ~5 km less vertical section of rock removed in the western portion of the EC than on the eastern side. However, Figure 6 shows good agreement between the upper limit of the cross section estimate, point estimates of exhumation taken from the cross section and reset ZFT and ^{40}Ar/^{39}Ar ages.

[72] Erosion estimates from the cross section are greater than that given by the AFT thermochronology in the IA (Table 3). Part of this apparent discrepancy may be in the low-temperature range of the available thermochronometers. All AFT samples are reset, with most of the maximum component ages being Tertiary [*Barnes et al.*, 2006]. Also, the 3–5 km of structural overlap depicted above the surface (Foldout 2) in the IA may have never been expressed as burial if erosion kept pace with the motion on the fault. Thus removal of material was lateral verses vertical making the

Table 4. Comparison of Exhumation Estimates Across Andean Fold-Thrust Belt

	Location	EC[a]	IA	SA	Total	Length	Average Magnitude
North	(15°–17°S)	891–1610	194–295	35–310[b]	1120–2013	300	4–7
South[c]	(20°S)	725–1285	347–640	192–432	1264–2357	380	3–6

[a]EC, IAZ, SAZ, and total exhumation estimate are in kilometers squared.
[b]Thickness of eroded Tertiary sediments is assumed to be 4 km in this portion of the SAZ, reflecting greater magnitudes of preserved Tertiary rocks in this region. In all other parts of the FTB in the north and south the thickness of eroded Tertiary sediments is assumed to be 3 km.
[c]Data from *Barnes and Pelletier* [2006] and *Barnes et al.* [2008].

integrated ''vertical'' amount of exhumation an overestimate. The point estimates that fall between the thermochronometer derived and averaged cross section exhumation estimates also support laterally removed material (Figure 6b).

[73] In the SA, the upper end of denudation estimates based on the cross sections matches the lower end of the thermochronometer exhumation estimates (Table 3). The upper estimate assumes 4 km of Tertiary basin fill prior to deformation, which, for the Subandes, was most likely the case. Also, more than any other part of the fold-thrust belt, the regional estimates for the SA will underestimate exhumation magnitudes on the uplifted hanging wall of SA thrusts. Point estimates of erosion from thrusts closely match the thermochronometer exhumation estimate derived from the same location (Figure 6b). Thus, the upper end of the averaged cross-section estimate (3–4 km) is the most appropriate one to compare to the 3–5 km thermochronometer based estimate.

7. Conclusions

[74] This study presents new structural and thermochronometer observations across a 300-km width of the central Andean fold-thrust belt in northern Bolivia at 15–17°S. Thermochronometer samples were interpreted in the context of the neighboring structures and tectonic history. This coupling of thermochronology with balanced sections provided age constraints on the timing of deformation in the central Andes. The primary conclusions of this study include the following:

[75] 1. Total magnitude of shortening is 276 km, 30–60 km less than sections to the south. Percent shortening is 40%, essentially equal to that in central (40%) and southern (37%) Bolivia.

[76] 2. New orogen-wide shortening estimates in addition to a suite of mineral cooling ages indicate that the majority of shortening in the central Andes (~60%) is focused in the Eastern Cordillera (44%) and Interandean zone (17%) and is predominantly pre-Neogene (~45–25 Ma). Shortening in the Subandes accounts for 24% of the total shortening budget and is the locus of deformation since ~15 Ma.

[77] 3. Compiled new and previous fission track thermochronology of the Eastern Cordillera and Interandean zone suggest that both regions experienced two phases of cooling via erosion: (1) an earlier phase in the EC from late Eocene to Oligocene (~25–40 Ma; recorded by ZFT and $^{40}Ar/^{39}Ar$ data) and in the IA more poorly constrained, initiating in the late Oligocene (≥~25 Ma; recorded by AFT data) at the latest, and (2) both regions experienced a later phase starting in the mid-late Miocene until present (~15–0 Ma). Furthermore, the EC back thrust zone in the Rio La Paz drainage experienced Plio-Quaternary cooling (~2–5 Ma; recorded by AFT data) probably via recent fluvial incision. However, this exhumation in the western EC has been insufficient to reset a single ZFT cooling age showing substantial local variation in the magnitude of northern EC exhumation.

[78] 4. Rates of deformation are as high as 7 mm/a from ~50–25 Ma and vary between 4 to 8 mm/a in the Subandes depending if deformation initiates as early as 15 Ma or as late as 8 Ma. The combined cooling ages in northern Bolivia suggest a hiatus in cooling for 10–17 Ma between 25 and 15 or 8 Ma that we relate to a pause or a dramatic deceleration in the rate of deformation and propagation of the Andean fold-thrust belt over that same time period.

[79] 5. Both the large-scale structural geometries and the progressive kinematic evolution are consistent with the eastward propagation of large-scale basement thrust faults. Regional trends of mineral cooling ages suggest these basement thrusts sheets had the largest effect over the magnitude and location of exhumation. Movement on individual thrusts is not recorded by cooling within the Eastern Cordillera or Interandean zone.

Appendix A: Analytical Procedure Details

[80] The mineral separations and fission track analysis was performed by Apatite to Zircon, Inc. using standard heavy liquid techniques. Apatite grains were immersed in an epoxy resin that was cured at 90°C for 1 h. The cured mounts were polished to expose grain surfaces, followed by etching in 5.5N HNO_3 for 20.0 s (±0.5 s) at 21°C (±1°C) to reveal natural fission tracks. Zircon grains were mounted in FEP Teflon. The zircon mounts were also polished followed by immersion in a eutectic melt of $NaOH^{+}KOH$ at ~210°C (±10°C) for ~37 h and 10 min to adequately reveal naturally occurring fission tracks.

[81] All previous fission track ages from the study area were determined using the external detector method. The samples presented here used the laser ablation (LA-ICPMS) method of [*Donelick et al.*, 2005; *Hasebe et al.*, 2004]. Spontaneous tracks were first counted in unpolarized light at 2000x magnification. The LA-ICPMS was then used to determine the ^{238}U concentrations by measuring the ratio of ^{238}U to ^{43}Ca for apatite and ^{238}U to ^{29}Si for zircon, from the same grain regions where the spontaneous tracks were counted. Fission track ages were calculated using (1) the ratio of the number of fission tracks present in the grain to the amount of ^{238}U present and (2) a modified version of the radioactive decay equation that includes a LA-ICPMS zeta calibration factor [*Donelick et al.*, 2005]. The age standards used to calculate the zeta factor were (1) Durango apatite (30.6 ± 0.3 Ma) from Cerro de Mercado, Mexico, and (2) Fish Canyon zircon (27.9 ± 0.7 Ma) from the San Juan Mountains, Colorado.

[82] Following age analysis, the apatites were irradiated using ^{252}Cf to enhance the measurability of natural fission tracks [*Donelick and Miller*, 1991]. The irradiated grain mounts were reimmersed in 5.5N HNO_3 for 20.0 s (±0.5 s) at 21°C (±1°C) to reveal any horizontal, confined fission tracks, and the lengths subsequently measured. Track length and crystallographic orientation were recorded. For each grain age and track length a mean Dpar value was determined from 1 to 4 measurements.

Appendix B: Thermal Modeling Details

[83] We conducted inverse thermal modeling of the AFT data with HeFTy (beta version 6) [*Ehlers et al.*, 2005;

Ketcham, 2005]. We employed the annealing model of *Ketcham et al.* [1999] and the C axis projection model of *Ketcham* [2003] with the Cf irradiation option activated. For the age data, we used the 2σ uncertainty mode and the LA-ICPMS ratio method. For the length data, we used the track length and angle to c axis data and employed the default Kuiper's statistic method for calculating goodness of fit because the track length distributions tend to have significant tails. Default merit values of good (0.5) and acceptable (0.05) fits were used for the thermal histories. For both ages and track lengths, the kinetic parameter, Dpar, was also included. Only one kinetic population was designated that encompassed all of the age and track data in each sample. Initial, open-ended models used minimal constraints with a starting temperature of 200°C at an age equal to 50 Ma older than the depositional age and a 20°C present temperature. More refined modeling utilized those constraints, as well as additional geologic constraints, such as a 10–30°C temperature equal to the depositional age, and a fixed 50–180°C constraint equal in age to either (1) the 2σ range in concordant pooled age or (2) between the sample depositional age and 1 Ma for discordant samples to allow for the maximum flexibility in attempted thermal history paths explored. Thermal history segments were designated as episodic style, monotonic, and random spacing with halved 5 times (5E) to provide optimal flexibility in the attempted cooling paths between constraints. A 40°C/Ma maximum cooling/heating rate was imposed on all segments to limit the temperature histories to what is geologically reasonable. Models were run with a Monte Carlo search and 50,000 attempted paths.

[84] **Acknowledgments.** We thank Segeotechmin of La Paz Bolivia and especially Sohrab Tawackoli for logistical support. We have benefited from discussions and field observations from Peter DeCelles, Bobby Gillis, Brian Horton, and Andrew Leier. Reviews by Carmala Garzoine, Eric Kirby, Andrew Meigs, and an anonymous reviewer greatly improved the clarity and presentation of the manuscript. Support for this work was provided to T. A. Ehlers by NSF grant EAR 0409289.

References

Aalto, R., T. Dunne, and J. L. Guyot (2006), Geomorphic controls on Andean denudation rates, *J. Geol.*, *114*, 85–99, doi:10.1086/498101.

Avouac, J.-P., and E. B. Burov (1996), Erosion as a driving mechanism of intracontinental mountain growth, *J. Geophys. Res.*, *101*, 17,747–17,769, doi:10.1029/96JB01344.

Babeyko, A. Y., S. V. Sobolev, T. Vietor, O. Oncken, and R. B. Trumbull (2006), Numerical study of weakening processes in the central Andean back-arc, in *The Andes: Active Subduction Orogeny*, edited by O. Oncken et al., pp. 495–512, Springer, New York.

Baby, P., I. Moretti, B. Guillier, R. Limachi, E. Mendez, J. Oller, and M. Specht (1995), Petroleum system of the north and central Sub-Andean zone, in *Petroleum Basins of South America*, edited by A. J. Tankard, R. Suárez Soruco, and H. J. Welsink, *AAPG Mem.*, *62*, 445–458.

Baby, P., P. Rochat, G. Mascle, and G. Herail (1997), Neogene shortening contribution to crustal thickening in the back arc of the central Andes, *Geology*, *25*, 883–886, doi:10.1130/0091-7613(1997)025<0883:NSCTCT>2.3.CO;2.

Bally, A. W., P. L. Gordy, and G. A. Stewart (1966), Structure, seismic data, and orogenic evolution of southern Canadian Rocky Mountains, *Bull. Can. Pet. Geol.*, *14*, 337–381.

Barnes, J. B., and J. D. Pelletier (2006), Latitudinal variations of denudation in the evolution of the Bolivian Andes, *Am. J. Sci.*, *306*, 1–31, doi:10.2475/ajs.306.1.1.

Barnes, J. B., T. A. Ehlers, N. McQuarrie, P. B. Sullivan, and J. D. Pelletier (2006), Eocene to recent variations in erosion across the central Andean fold-thrust belt, northern Bolivia: Implications for plateau evolution, *Earth Planet. Sci. Lett.*, *248*, 118–133, doi:10.1016/j.epsl.2006.05.018.

Barnes, J. B., T. A. Ehlers, N. McQuarrie, P. B. O'Sullivan, and S. Tawackoli (2008), Thermochronometer record of central Andean plateau growth, Bolivia (19.5°S), *Tectonics*, doi:10.1029/2007TC002174, in press.

Beach, A. (1981), Thrust tectonics in the eastern Dauphinois Zone (French Alps), north of the Pelvoux massif, *J. Struct. Geol.*, *3*, 299–308, doi:10.1016/0191-8141(81)90026-2.

Beaumont, C., P. Fullsack, and J. Hamilton (1992), Erosional control of active compressional orogens, in *Thrust Tectonics*, edited by K. McClay, pp. 1–18, Chapman and Hall, London.

Beck, S. L., and G. Zandt (2002), The nature of orogenic crust in the central Andes, *J. Geophys. Res.*, *107*(B10), 2230, doi:10.1029/2000JB000124.

Benjamin, M. T. (1986), Fission track ages on some Bolivian plutonic rocks; implications for the Tertiary uplift and erosion history of the Altiplano-Cordillera Real, Master's thesis, 58 pp., Dartmouth Coll., Hanover, N. H.

Benjamin, M. T., N. M. Johnson, and C. W. Naeser (1987), Recent rapid uplift in the Bolivian Andes: Evidence from fission-track dating, *Geology*, *15*, 680–683, doi:10.1130/0091-7613(1987)15<680:RRUITB>2.0.CO;2.

Boyer, S. E., and D. Elliott (1982), Thrust systems, *AAPG Bull*, *66*, 1196–1230.

Brandon, M. T., M. Roden-Tice, and J. Garver (1998), Late Cenozoic exhumation of the Cascadia accretionary wedge in the Olympic Mountains, northwest Washington State, *Geol. Soc. Am. Bull.*, *110*, 985–1009, doi:10.1130/0016-7606(1998)110<0985:LCEOTC>2.3.CO;2.

Burtner, R. L., A. Nigrini, and R. A. Donelick (1994), Thermochronology of lower Cretaceous source rocks in the Idaho-Wyoming thrust belt, *AAPG Bull.*, *78*, 1613–1636.

Butler, R. W. H. (1983), Balanced cross-sections and their implications for the deep structure of the NW Alps, *J. Struct. Geol.*, *5*, 125–138, doi:10.1016/0191-8141(83)90038-X.

Crough, S. T. (1983), Apatite fission-track dating of erosion in the eastern Andes, Bolivia, *Earth Planet. Sci. Lett.*, *64*, 396–397, doi:10.1016/0012-821X(83)90099-7.

Dahlen, F. A., and J. Suppe (1988), Mechanics, growth, and erosion of mountain belts, in *Processes in Continental Lithospheric Deformation*, edited by S. P. Clark Jr., *Spec. Pap. Geol. Soc. Am.*, *218*, 161–178.

Dahlstrom, C. D. A. (1969), Balanced cross sections, *Can. J. Earth Sci.*, *6*, 743–757.

DeCelles, P. G., D. M. Robinson, J. Quade, T. P. Ojha, C. N. Garzione, P. Copeland, and B. N. Upreti (2001), Stratigraphy, structure, and tectonic evolution of the Himalayan fold-thrust belt in western Nepal, *Tectonics*, *20*, 487–509, doi:10.1029/2000TC001226.

Diegel, F. A. (1986), Topological constraints on imbricate thrust networks, examples from the Mountain City window, Tennessee, USA, *J. Struct. Geol.*, *8*, 269–279, doi:10.1016/0191-8141(86)90048-9.

Donelick, M. (1993), A method of fission track analysis utilizing bulk chemical etching of apatite, U.S. patent 5,267,274, U.S. Patent Off., Washington, D. C.

Donelick, M., and D. Miller (1991), Enhanced TINT fission track densities in low spontaneous track density apatites using 252Cf-derived fission fragment tracks: A model and experimental observations, *Nucl. Tracks Radiat. Meas.*, *18*, 301–307, doi:10.1016/1359-0189(91)90022-A.

Donelick, R. A., P. B. O'Sullivan, and R. A. Ketcham (2005), Apatite fission-track analysis, in *Low-Temperature Thermochronology: Techniques, Interpretations, and Applications*, *Rev. Mineral. Geochem.*, vol. 58, edited by P. W. Reiners, and T. A. Ehlers, pp. 49–94, Mineral. Soc. of Am., Washington, D. C.

Dorbath, C., and M. Granet (1996), Local earthquake tomography of the Altiplano and the Eastern Cordillera of northern Bolivia, *Tectonophysics*, *259*, 117–136, doi:10.1016/0040-1951(95)00052-6.

Dorbath, C., M. Granet, G. Poupinet, and C. Martinez (1993), A teleseismic study of the Altiplano and the Eastern Cordillera in northern Bolivia—New constraints on a lithospheric model, *J. Geophys. Res.*, *98*, 9825–9844, doi:10.1029/92JB02406.

Dunne, T., L. A. K. Mertes, R. H. Meade, J. E. Richey, and B. R. Forsberg (1998), Exchanges of sediment between the flood plain and the channel of the Amazon River in Brazil, *Geol. Soc. Am. Bull.*, *110*, 450–467, doi:10.1130/0016-7606(1998)110<0450:EOSBTF>2.3.CO;2.

Echavarria, R., R. Hernandez, R. W. Allmendinger, and J. H. Reynolds (2003), Subandean thrust and fold belt of northwest Argentina: Geometry and timing of the Andean evolution, *AAPG Bull.*, *87*, 965–985, doi:10.1306/01200300196.

Ege, H., E. R. Sobel, V. Jacobshagen, E. Scheuber, and D. Mertmann (2003), Exhumation history of the central Andes of southern Bolivia by apatite fission track dating, *Rev. Tec. YPFB*, *21*, 165–172.

Ege, H., E. R. Sobel, E. Scheuber, and V. Jacobshagen (2007), Exhumation history of the southern Altiplano plateau (southern Bolivia) constrained by apatite fission track thermochronology, *Tectonics*, *26*, TC1004, doi:10.1029/2005TC001869.

Ehlers, T. A. (2005), Crustal thermal processes and the interpretation of thermochronometer data, in *Low-Temperature Thermochronology: Techniques, Interpretations, and Applications*, *Rev. Mineral. Geochem.*, vol. 58, edited by P. W. Reiners, and T. A. Ehlers, pp. 315–350, Mineral. Soc. of Am., Washington, D. C., doi:10.2138/rmg.2005.58.12.

Ehlers, T. A., et al. (2005), Computational tools for low-temperature thermochronometer interpretation, in *Low-Temperature Thermochronology: Techniques, Interpretations, and Applications*, *Rev. Mineral. Geochem.*, vol. 58, edited by P. W. Reiners, and T. A. Ehlers, pp. 589–622, Mineral. Soc. of Am., Washington, D. C.

Elger, K., O. Oncken, and J. Glodny (2005), Plateau-style accumulation of deformation: Southern Altiplano, *Tectonics*, *24*, TC4020, doi:10.1029/2004TC001675.

Elliott, D. (1983), The construction of balanced cross-sections, *J. Struct. Geol.*, *5*, 101, doi:10.1016/0191-8141(83)90035-4.

Fitzgerald, P. G., R. B. Sorkhabi, T. F. Redfield, and E. Stump (1995), Uplift and denudation of the central Alaska Range: A case study in the use of apatite fission track thermochronology to determine absolute uplift parameters, *J. Geophys. Res.*, *100*, 20,175–20,191, doi:10.1029/95JB02150.

Galbraith, R. F. (1981), On statistical models for fission-track counts, *J. Math. Geol.*, *13*, 471–478, doi:10.1007/BF01034498.

Galbraith, R. F. (2005), *Statistics for Fission Track Analysis*, 219 pp., CRC, Boca Raton, Fla.

Garzione, C. N., P. Molnar, J. C. Libarkin, and B. J. MacFadden (2006), Rapid late Miocene rise of the Bolivian Altiplano: Evidence for removal of mantle lithosphere, *Earth Planet. Sci. Lett.*, *241*, 543–556, doi:10.1016/j.epsl.2005.11.026.

Gillis, R. J., B. K. Horton, and M. Grove (2006), Thermochronology, geochronology, and upper crustal structure of the Cordillera Real: Implications for Cenozoic exhumation of the central Andean plateau, *Tectonics*, *25*, TC6007, doi:10.1029/2005TC001887.

Gonzalez, M., E. Diaz-Martinez, and L. Ticlla (1996), Comentarios sobre la estratigraphia del Silurico y Devonico del norte y centro de la Cordillera Oriental y Altiplano de Bolivia, paper presented at Simposio Sul Americano do Siluro-Devoniano, Anais, Ponta Grossa, Brazil.

Green, P. F. (1981), A new look at statistics in fission-track dating, *Nucl. Tracks Radiat. Meas.*, *5*, 77–86, doi:10.1016/0191-278X(81)90029-9.

Guarachi, H. P., S. Tawackoli, W. A. Salinas, and H. M. Gonzales (2001), Mapa Geologico de Bolivia, scale 1:1,000,000, Serv. Geol. de Bolivia/Yacimientos Petrol. Fiscals Bolivianos, La Paz.

Hasebe, N., J. Barbarand, K. Jarvis, A. Carter, and A. J. Hurford (2004), Apatite fission-track chronometry using laser ablation ICP-MS, *Chem. Geol.*, *207*, 135–145, doi:10.1016/j.chemgeo.2004.01.007.

Hatcher, R. D., Jr. (2004), Properties of thrusts and the upper bounds for the size of thrust sheets, in *Thrust Tectonics and Hydrocarbon Systems*, edited by K. R. McClay, *AAPG Mem.*, *82*, 18–29.

Hatcher, R. D., and R. J. Hooper (1992), Evolution of crystalline thrust sheets in the internal parts of mountain chains, in *Thrust Tectonics*, edited by K. R. McClay, pp. 217–233, Chapman and Hall, London.

Hodges, K., C. Wobus, K. Ruhl, T. Schildgen, and K. X. Whipple (2004), Quaternary deformation, river steepening, and heavy precipitation at the front of the Higher Himalayan ranges, *Earth Planet. Sci. Lett.*, *220*, 379–389, doi:10.1016/S0012-821X(04)00063-9.

Horton, B. K. (1998), Sediment accumulation on top of the Andean orogenic wedge: Oligocene to late Miocene basins of the Eastern Cordillera, southern Bolivia, *Geol. Soc. Am. Bull.*, *110*, 1174–1192. (Erratum, *Geol. Soc. Am. Bull.*, *110*, 1513.)

Horton, B. K. (1999), Erosional control on the geometry and kinematics of thrust belt development in the central Andes, *Tectonics*, *18*, 1292–1304, doi:10.1029/1999TC900051.

Horton, B. K. (2005), Revised deformation history of the central Andes: Inferences from Cenozoic foredeep and intermontane basins of the Eastern Cordillera, Bolivia, *Tectonics*, *24*, TC3011, doi:10.1029/2003TC001619.

Horton, B. K., and P. G. DeCelles (1997), The modern foreland basin system adjacent to the central Andes, *Geology*, *25*, 895–898, doi:10.1130/0091-7613(1997)025<0895:TMFBSA>2.3.CO;2..

Horton, B. K., B. A. Hampton, and G. L. Waanders (2001), Paleogene synorogenic sedimentation in the Altiplano Plateau and implications for initial mountain building in the central Andes, *Geol. Soc. Am. Bull.*, *113*, 1387–1400, doi:10.1130/0016-7606(2001)113<1387:PSSITA>2.0.CO;2.

Horton, B. K., B. A. Hampton, B. N. LaReau, and E. Baldellon (2002), Tertiary Provenance history of the northern and central Altiplano (central Andes, Bolivia): A detrital record of plateau-margin tectonics, *J. Sediment. Res.*, *72*, 711–726, doi:10.1306/020702720711.

Isacks, B. L. (1988), Uplift of the central Andean Plateau and bending of the Bolivian Orocline, *J. Geophys. Res.*, *93*, 3211–3231, doi:10.1029/JB093iB04p03211.

Kay, R. F., B. J. MacFadden, R. H. Madden, H. Sandeman, and F. Anaya (1998), Revised age of the Salla beds, Bolivia, and its bearing on the age of the Deseadan South American land mammal "age", *J. Vertebrate Paleontol.*, *18*, 189–199.

Ketcham, R. A. (2003), Observations on the relationship between crystallographic orientation and biasing in apatite fission-track measurements, *Am. Mineral.*, *88*, 817–829.

Ketcham, R. A. (2005), Forward and inverse modeling of low-temperature thermochronometry data, in *Low-Temperature Thermochronology: Techniques, Interpretations, and Applications*, *Rev. Mineral. Geochem.*, vol. 58, edited by P. W. Reiners and T. A. Ehlers, pp. 278–314, Mineral. Soc. of Am., Washington, D. C.

Ketcham, R. A., R. A. Donelick, and W. D. Carlson (1999), Variability of apatite fission-track annealing kinetics; III, Extrapolation to geological time scales, *Am. Mineral.*, *84*, 1235–1255.

Kley, J. (1996), Transition from basement-involved to thin-skinned thrusting in the Cordillera Oriental of southern Bolivia, *Tectonics*, *15*, 763–775, doi:10.1029/95TC03868.

Kley, J. (1999), Geologic and geometric constraints on a kinematic model of the Bolivian Orocline, in *Central Andean Deformation*, edited by K. J. Reutter, pp. 221–235, Pergamon, Oxford, U.K.

Lamb, S., and P. Davis (2003), Cenozoic climate change as a possible cause for the rise of the Andes, *Nature*, *425*, 792–797, doi:10.1038/nature02049.

Lamb, S., and L. Hoke (1997), Origin of the high plateau in the Central Andes, Bolivia, South America, *Tectonics*, *16*, 623–649, doi:10.1029/97TC00495.

MacFadden, B. J., F. Anaya, and C. C. Swisher (1995), Neogene paleomagnetism and oroclinal bending of the central Andes of Bolivia, *J. Geophys. Res.*, *100*, 8153–8167, doi:10.1029/95JB00149.

Masek, J. G., B. L. Isacks, T. L. Gubbels, and E. J. Fielding (1994), Erosion and tectonics at the margins of continental plateaus, *J. Geophys. Res.*, *99*, 13,941–13,956, doi:10.1029/94JB00461.

McQuarrie, N. (2002), The kinematic history of the central Andean fold-thrust belt, Bolivia: implications for building a high plateau, *Geol. Soc. Am. Bull.*, *114*, 950–963, doi:10.1130/0016-7606(2002)114<0950:TKHOTC>2.0.CO;2.

McQuarrie, N., and G. H. Davis (2002), Crossing the several scales of strain-accomplishing mechanisms: The central Andean fold-thrust belt, *J. Struct. Geol.*, *24*, 1587–1602, doi:10.1016/S0191-8141(01)00158-4.

McQuarrie, N., and P. DeCelles (2001), Geometry and structural evolution of the central Andean back thrust belt, Bolivia, *Tectonics*, *20*, 669–692, doi:10.1029/2000TC001232.

McQuarrie, N., B. K. Horton, G. Zandt, S. Beck, and P. G. DeCelles (2005), Lithospheric evolution of the Andean fold-thrust belt, Bolivia, and the origin of the central Andean plateau, *Tectonophysics*, *399*, 15–37, doi:10.1016/j.tecto.2004.12.013.

McRae, L. E. (1990), Paleomagnetic isochrons, unsteadiness, and uniformity of sedimentation in Miocene intermontane basin sediments at Salla, eastern Andean Cordillera, Bolivia, *J. Geol.*, *98*, 479–500.

Montgomery, D. R., G. Balco, and S. D. Willett (2001), Climate, tectonics, and the morphology of the Andes, *Geology*, *29*, 579–582, doi:10.1130/0091-7613(2001)029<0579:CTATMO>2.0.CO;2.

Morley, C. K. (1988), Out-of-sequence thrusts, *Tectonics*, *7*, 539–561.

Müller, J. P., J. Kley, and V. Jacobshagen (2002), Structure and Cenozoic kinematics of the Eastern Cordillera, southern Bolivia (21°S), *Tectonics*, *21*(5), 1037, doi:10.1029/2001TC001340.

Reiners, P. W., T. A. Ehlers, and P. K. Zeitler (2005), Past present and future of thermochronology, in *Low-Temperature Thermochronology: Techniques, Interpretations, and Applications*, *Rev. Mineral. Geochem.*, vol. 58, edited by P. W. Reiners and T. A. Ehlers, pp. 1–18, Mineral. Soc. of Am., Washington, D. C., doi:10.2138/rmg.2005.58.1.

Roeder, D. (1988), Andean-age structure of Eastern Cordillera (province of La Paz, Bolivia), *Tectonics*, *7*, 23–39, doi:10.1029/TC007i001p00023.

Roeder, D., and R. L. Chamberlain (1995), Structural geology of sub-Andean fold and thrust belt in northwestern Bolivia, in *Petroleum Basins of South America*, edited by A. J. Tankard, R. Suárez Soruco, and H. J. Welsink, *AAPG Mem.*, *62*, 459–479.

Safran, E. B. (1998), Channel network incision and patterns of mountain geomorphology, Ph.D. thesis, Univ. of Calif., Santa Barbara.

Safran, E. B., A. E. Blythe, and T. Dunne (2006), Spatially variable exhumation rates in orogenic belts: An Andean example, *J. Geol.*, *114*, 665–681, doi:10.1086/507613.

Scheuber, E., D. Mertmann, H. Ege, P. H. Silva-Gonzalez, C. Heubeck, K.-J. Reutter, and V. Jacobshagen (2006), Exhumation and basin development related to formation of the central Andean Plateau, 21°S, in *The Andes: Active Subduction Orogeny*, edited by O. Oncken, et al., pp. 285–301, Springer, New York.

Sempere, T. (1995), Phanerozoic evolution of Bolivia and adjacent regions, in *Petroleum Basins of South America*, edited by A. J. Tankard, R. Suárez Soruco, and H. J. Welsink, *AAPG Mem.*, *62*, 207–230.

Sempere, T., G. Herail, J. Oller, and M. G. Bonhomme (1990), Late Oligocene-early Miocene major tectonic crisis and related basins in Bolivia, *Geology*, *18*, 946–949, doi:10.1130/0091-7613(1990)018<0946:LOEMMT>2.3.CO;2.

Sempere, T., L. G. Marshall, S. Rivano, and E. Godoy (1994), Late Oligocene–early Miocene compressional tectosedimentary episode and associated land-mammal faunas in the Andes of central Chile and adjacent Argentina (32–37°S), *Tectonophysics*, *229*, 251–264, doi:10.1016/0040-1951(94)90032-9.

Servicio Geologico de Bolivia (GEOBOL) (1994a), Carta Geologica de Bolivia, Chulumani (Hoja 6044), scale 1:100,000, La Paz.

Servicio Geologico de Bolivia (GEOBOL) (1994b), Carta Geologica de Bolivia, Coroico (Hoja 6045), scale 1:100,000, La Paz.

Servicio Geologico de Bolivia (GEOBOL) (1995a), Carta Geologica de Bolivia, Calamarca (Hoja 5943), scale 1:100,000, La Paz.

Servicio Geologico de Bolivia (GEOBOL) (1995b), Carta Geologica de Bolivia, Milluni (Hoja 5945), scale 1:100,000, La Paz.

Servicio Geologico de Bolivia (GEOBOL) (1995c), Carta Geologica de Bolivia, Sapahaqui (Hoja 6043), scale 1:100,000, La Paz.

Servicio Geologico de Bolivia (GEOBOL) (1996), Mapas Tematicos de Recursos Minerales de Bolivia, Corocoro y Charana, scale 1:250,000, La Paz.

Servicio Geologico de Bolivia (GEOBOL) (1997), Mapas Tematicos de Recursos Minerales de Bolivia, La Paz y Copacabana, scale 1:250,000, La Paz.

Sobolev, S. V., A. Y. Babeyko, I. Koulakov, and O. Oncken (2006), Mechanism of the Andean orogeny: insight from numerical modeling, in *The Andes: Active Subduction Orogeny*, edited by O. Oncken et al., pp. 513–535, Springer, New York.

Srivastava, P., and G. Mitra (1994), Thrust geometries and deep structure of the outer and lesser Himalaya, Kumaon and Garhwal (India): Implications for evolution of the Himalayan fold-and-thrust belt, *Tectonics*, *13*, 89–109.

Stolar, D. B., S. D. Willett, and G. H. Roe (2006), Climate and ectonic forcing of a critical orogen, in *Tectonics, Climate and Landscape Evolution*, edited by S. D. Willett et al., *Spec. Pap. Geol. Soc. Am.*, *398*, 241–250.

Suarez, R., and E. Diaz (1996), Lexico estratigrafico de Bolivia, *Rev. Tec. Yacimientos Petrol. Fis. Bolivianos*, *17*(1–2), 7–227.

Tagami, T., and P. B. O'Sullivan (2005), Fundamentals of fission-track thermochronology, in *Low-Temperature Thermochronology: Techniques, Interpretations, and Applications*, *Rev. Mineral. Geochem.*, vol. 58, edited by P. W. Reiners and T. A. Ehlers, pp. 19–48, Mineral. Soc. of Am., Washington, D. C., doi:10.2138/rmg.2005.58.2.

Watts, A. B., S. H. Lamb, J. D. Fairhead, and J. F. Dewey (1995), Lithospheric flexure and bending of the central Andes, *Earth Planet. Sci. Lett.*, *134*, 9–21, doi:10.1016/0012-821X(95)00095-T.

Welsink, H. J., M. A. Franco, and G. C. Oviedo (1995), Andean and pre-Andean deformation, Boomerang Hills area, Boliva, in *Petroleum Basins of South America*, edited by A. J. Tankard, R. Suárez Soruco, and H. J. Welsink, *AAPG Mem.*, *62*, 481–499.

Willett, S. (1999), Orogeny and orography; the effects of erosion on the structure of mountain belts, *J. Geophys. Res.*, *104*, 28,957–28,982, doi:10.1029/1999JB900248.

Woodward, N. B., S. E. Boyer, and J. Suppe (1989), *Balanced Geological Cross-Sections: An Essential Technique in Geological Research and Exploration*, *Short Course Geol.*, vol. 6, AGU, Washington, D. C.

Zeitler, P. K., C. P. Chamberlain, and H. A. Smith (1993), Synchronous anatexis, metamorphism, and rapid denudation at Nanga Parbat (Pakistan Himalaya), *Geology*, *21*, 347–350, doi:10.1130/0091-7613(1993)021<0347:SAMARD>2.3.CO;2.

Zubieta Rossetti, D., P. Baby, and J. L. Mugnier (1996), Cenozoic evolution of the Andean foreland basin between 15°30′ and 22°00′, paper presented at Third International Symposium on Andean Geodynamics, ORTSTROM, St. Malo, France.

J. B. Barnes and T. A. Ehlers, Department of Geological Sciences, University of Michigan, Ann Arbor, MI 48109-1005, USA.

N. McQuarrie, Department of Geosciences, Princeton University, 207 Guyot Hall, Princeton, NJ 08544, USA. (nmcq@princeton.edu)